Cobalt ferrite spinel catalyst synthesized through a novel route for hydrogen generation from sodium borohydride hydrolysis

Tonetti, L. T.[1], Medeiros, M. S.[1], Liying Liu[3], Park, V. N.[4], Valente-Rodrigues, C. L.[5], Letichevsky, S.[2,6], Fajardo, H. V.[4], Navarro, R. C. S.[2], Maia, M. E. H.[7]

1. COPPE, PENt, Federal University of Rio de Janeiro, Rio de Janeiro, Rio de Janeiro, Brazil.
2. *Chemical and Materials Engineering Department, Pontifical Catholic University of Rio de Janeiro (PUC - Rio), Rio de Janeiro, Rio de Janeiro, Brazil.*
3. *Brazilian Center of Physical Research (CBPF), Rio de Janeiro, Rio de Janeiro, Brazil.*
4. *Chemistry Department, Federal University of Ouro Preto (UFOP), Minas Gerais, Ouro Preto, Brazil.*
5. *Physics institute, Federal University of Rio de Janeiro (UFRJ), Rio de Janeiro, Rio de Janeiro, Brazil.*
6. *New Wave Tech, Chácara Rio – Petrópolis, Duque de Caxias, Rio de Janeiro, Rio de Janeiro, Brazil.*
7. *Physics Department*, *Pontifical Catholic University of Rio de Janeiro (PUC - Rio), Rio de Janeiro, Rio de Janeiro, Brazil.*

Abstract:

Stimulated through energy concerns and life preservation necessity in our planet, new and greener energy resources have been searched to reduce the emission of greenhouse gases. In this scenario, hydrogen appears as a viable clean energy source. Sodium borohydride ($NaBH_4$) is an auspicious hydrogen carrier due to its high hydrogen density value (10.8% w/v.), safe manipulation and fast kinetics of pure hydrogen release. In order to efficiently extract the H_2 confided inside $NaBH_4$ solution, a proper catalyst must be added, which can be of heterogeneous nature. In the present work, a new cobalt ferrite spinel ($CoFe_2O_4$) containing catalyst was produced through a novel chemical route based on metal adsorption over nanocellulose fibers (TCNF), which act as reactive templates during solid phase (TCNF impregnated with metallic cations) calcination under air.

The obtained material was next tested for its catalytic activity regarding H_2 production through basic $NaBH_4$ aqueous solutions for a temperature range between 10 and 55 °C. After Rietveld analysis, catalyst sample revealed to be comprised of 74.8% w/w of the spinel phase ($CoFe_2O_4$), 25 % w/w of Hematite (Fe_2O_3) and 0.2% w/w of iron sulfate ($Fe_2(SO_4)_3$). Microscopy analysis indicated the presence of agglomerations of particles with spheroidal shape and particle size in the range between 15 and 20 nm. Additionally, EDS maps indicated a homogeneous distribution of iron and cobalt inside the cobalt ferrite particles. Results from performed H_2 generation study indicated a promising catalytic behavior, with 1785 mL of H_2 being produced during only 15 min reaction at 25°C for 50 mg of catalyst and initial concentrations of $NaBH_4$ and NaOH respectively equal to 4.0% and 2.5% w/v. The amount of H_2 produced is close to the maximum value allowed through stoichiometric considerations under the proposed conditions (2086 mL). Specific hydrogen generation rate (HGR) showed a maximum value of 3.55 L min^{-1} g_{cat}^{-1} at 40 °C, with activation energies determined through an empirical power law and Langmuir – Hischelwood (L-H) models respectively equal to 38.4 ± 5.3 of 42.2 ± 5.8 kJ mol^{-1} (10 to 55°C), both in the range of previously reported values for other cobalt ferrite containing materials. Kinetic data was better fitted to the L - H model, which is consistent with the fact that during hydrolysis, adsorption of boron complexes over catalyst surface should occur prior to H_2 evolution.

Key words: Hydrogen, TCNF, Fe_2CoO_4, $NaBH_4$, Langmuir – Hischelwood.

Introduction

On the last decade, encouraged by their direct impact on climate change, greenhouse gases emission has become a global problem. In order to minimize it, the search for other and greener energy resources must be stimulated, thereby contributing to reduce the rate of mean planet temperature rise [1–3]. Despite the possibility of the visible potential of solar and wind energy generation, they are influenced by climate conditions, and therefore, are submitted to considerable seasonality, which may delay the energy generation, considering a whole electrical system [4].

On the other hand, hydrogen can be considered a great renewable energy source. Understood by the multiple synthesis routes and the sole production of water during its oxidation. However, gaseous, or liquid H_2 storage brings relevant technological issues, which have continuously stimulated the search of efficient new storage and extraction strategies, such as production of borohydrides, $NaBH_4$, followed by dissolution in water under basic pH.

Besides the fact that hydrogen can be generated through multiple green processes, for example, through water splitting or hydrocarbon reforming, energy production based on H_2 oxidation should result in water as the sole product [5,6]. However, H_2 storage brings important technological concerns, stimulated by the difficulty of hindering diffusion, when confined as a gas or liquid under pressure. In order to solve this issue a possible strategy is defined by different ways of obtaining hydrogen gas, such as hydrocarbons separation using heating, natural gas, and also through hydrolysis of metal-boron hydrides [7–9].

Due to its stability in basic aqueous solutions and high hydrogen storage content, sodium borohydride is a promising source for hydrogen generation. When $NaBH_4$ is present in aqueous solution under a neutral pH, it is observed that H_2 evolution spontaneously occurs, although with a slow kinetics at room temperature [8,10]. Therefore, in order to inhibit H_2 formation, addition of a strong base, such as NaOH, enhances solution pH, stabilizing the borohydride through formation of boron complexes with the available OH^- anions [11]. Addition of a proper catalyst then enables the controlled release of H_2 under a satisfactory rate [12]. Under the presence of a suitable oxide catalyst, for example, $NaBH_4$ hydrolysis process can be globally described by equation (1) [13].

According to literature, as long as boron hydride is still available, H_2 evolution should develop irreversibly. Moreover, around half of the obtained hydrogen comes from water splitting [8], suggesting a non-elementary reaction mechanism.

$$NaBH_{4(aq)} + 2H_2O_{(l)} \rightarrow NaBO_{2(aq)} + 4H_{2(g)} \quad (1)$$

Catalytic hydrolysis of sodium borohydride in basic aqueous solutions, can be achieved by two main ways: homogeneous or heterogeneous catalysis. In the first one, the catalyst and the reactants are in the same phase. Therefore, the separation of catalyst and reaction medium is difficult, which results in higher processing costs. On the other hand, heterogeneous catalysis solves the separation problem, because reaction medium and solid catalyst are in different physical states, specially, when the catalyst crystals are magnetic, making separation even easier. This is the case of cobalt ferrite spinel ($CoFe_2O_4$) containing materials, as will be shown later in present study.

In this context, noble metal-based materials have attracted considerable attention due to its high catalytic activity, however, considerable costs are usually involved during synthesis [10,14–19]. To handle this problem, non-metal-based catalysts, for example, alloys or oxides, can be viewed as interesting alternatives [12]. Cobalt-based catalysts, for example, have been intensively studied in the last years, which can be justified by metal precursor availability, lower production costs, and also the possibility of achieving similar performances when compared with noble metal containing catalysts [20,21].

Liu and Li synthesized Co-B nanoparticles using $CoCl_2$ and $NaBH_4$ in aqueous media as precursors and studied the H_2 evolution kinetics from $NaBH_4$ aqueous solutions. Catalyst morphology was described as an aggregate of spherical particles with an average size between 10 and 50 nm. The catalyst performance was 26 L H_2 min^{-1} g^{-1}, for 15% w/v $NaBH_4$ and 5% w/v NaOH, both dissolved in 20 mL of H_2O. Additionally, reaction kinetics was first order, for an initial NaOH concentration of 0.075 mol L^{-1} [22].

Balčiūnaitė et al. [23] synthesized different metallic cobalt containing catalysts for H_2 generation from sodium borohydride aqueous solutions. During synthesis electroless deposition of different metals (Co, Mo, Mn, Zn and Fe) and boron in cooper matrix sheets was performed. Authors used sulfate metal precursors, mixed with morpholine borane, used as a reducing agent, under pH of 7.0, under a fixed temperature, which varied between 30 and 60ºC, depending on sample nature. The produced alloys were next tested for their catalytic activity during sodium borohydride hydrolysis and through kinetic modelling of measured H_2 evolution rates, global activation energy then estimated. Global activation energy varied between 27 kJ.mol^{-1} (CoBMo/Cu) and 74 kJ.mol^{-1} (CoFeB/Cu). Authors evidenced that the highest hydrogen generation rate was 53.5 mL min^{-1} at 343 K for CoBMo/Cu in a solution containing initial concentrations of 5% w/v and 0.4 w/v for $NaBH_4$ and NaOH, respectively, using 15 mL of distilled water. These results reinforce the potential associated with cobalt containing catalysts towards sodium borohydride hydrolysis, also reflected in the high number of publications in these field [20,24–27].

In the work of Sahin et al. (2017) [28], Co-B-P particles were used as catalyst for $NaBH_4$ hydrolysis in basic media. Best results were achieved with plasma treated samples, which, for 25 mg catalyst at 30°C, 2.5% $NaBH_4$ (w/w) and 3.0% NaOH (w/w) initial concentrations, resulted in a maximum H_2 volume around 700 mL for a reaction time of approximately 12.6 min. The HGR value found at these conditions has shown to be equal to 3.98 $L.min^{-1}.g^{-1}$.

Besides use of metallic cobalt containing catalysts, some research was also performed regarding use of oxides, including iron cobalt spinel containing materials. For example, in the work of Abdelhamid (2021) [29], zirconium oxysulfate samples containing a carbonaceous phase ($ZrOSO_4$/C) were tested. Best results were reported for catalyst produced with 50% (w/w) of sulfuric acid, which, for an initial $NaBH_4$ concentration of 3% (m/V), enabled generation of a maximum H_2 volume of 500 mL, for an astonishing reaction time around 3 min. However, temperature and catalyst amount employed were not informed by the author. In the work of Saka et al. (2021) [30], a composite material of kaolin-clay functionalized with acetic acid and CoB particles was tested as catalyst for $NaBH_4$ hydrolysis, at 30°C, 5% (m/v) $NaBH_4$ and 1% (m/v) NaOH initial concentrations. For 100 mg catalyst at these conditions, a maximum amount of H_2 of 1,3 L was produced after 40 min, with an impressive HGR of 1,533 $L.min^{-1}.g^{-1}$.) for an expressive borohydride concentration of 18.9% (w/w). Also, cobalt alloy nanoparticles have shown catalytic activity for H_2 generation from $NaBH_4$ hydrolysis. In the work of Didebahn et al. (2018) [31], cobalt – nickel bimetallic nanoparticles supported in activated carbon were tested as catalyst for $NaBH_4$ hydrolysis for initial concentrations of boronhydride and NaOH both equal to 5 % (w/w).

Best results were achieved at 30ºC for the sample containing a cobalt to nickel proportion of 3:1 (highest cobalt mol fraction tested), with a HGR of 658.8 $L.min^{-1}.g^{-1}$. Besides metallic catalysts, nano-oxides have also been applied for H_2 production through $NaBH_4$ hydrolysis, showing a promising activity, specially for cobalt oxide bearing materials.

In the work of Durano et al. (2017) [32], for example, Co_3O_4 nanorods, synthesized by modified urea precipitation method, were tested as catalyst for $NaBH_4$ hydrolysis reaction. For 0,6 % $NaBH_4$ (w/w) and 0,12 % Co_3O_4 (w/w) initial concentrations (calculated with reference to a water volume of 50 mL) at 25ºC, a maximum amount of H_2 of approximately 750 mL was generated for a reaction time of 7 min, with a HGR value of 1.78 $L.min^{-1}.g^{-1}$. In the work of Javarzadeh et al. (2022) [33], a nanocomposite comprised of cobalt ferrite ($CoFe_2O_4$) anchored in a doped (nitrogen and sulfur) graphene structure was employed as catalyst for $NaBH_4$ hydrolysis. A prominent catalytic activity was evidenced for 20 mg catalyst at 25ºC for an initial concentration of $NaBH_4$ equal to 3.8 % (w/w) and pH equal to 10, with a maximum HGR of 8.5 $L.min^{-1}.g^{-1}$. Also, the synthesized catalyst showed an appreciable chemical stability, retaining almost 95% of the initial activity after five reaction cycles, suggesting that the carbon bearing phase acted as a protection against chemical interactions with the aggressive chemical surroundings. In the work of Karani and Fathirad (2023) [34], cobalt ferrite nanoparticles adhered to the surface of oxidized graphene nanoribbons were tested as a possible catalyst for $NaBH_4$ hydrolysis. Optimum H_2 production was achieved at 35ºC for 15 mg catalyst and initial concentrations of NaOH and $NaBH_4$ equal to 2.0 % (w/w). Under these conditions, HGR achieved an expressive value of 3.7 $L.min^{-1}.g^{-1}$.

Catalytic performance of spinels can be optimized through proper metallic doping. In the work of Deonikar et al. (2020) [35], nano particles of a cobalt molybdenum spinel ($CoMoO_4$) were doped with cooper ($Co_xCu_{1-x}MoO_4$) and its catalytic activity for $NaBH_4$ hydrolysis under basic conditions then tested. For x equal to 0.1, a promising HGR of 1.01 $L.min^{-1}.g^{-1}$ was achieved at 25°C for 30 mg catalyst and 50 mg $NaBH_4$. Reaction kinetics was described through a first order empirical model (R^2 = 0.9896), and a global activation energy of 30.8 $kJ.mol^{-1}$ was revealed. Catalyst reuse was also investigated, and low variation of maximum H_2 produced in five consecutive reaction cycles was evidenced (around 600 mL for the first cycle and 500 mL for the fifth cycle).

It is worthwhile to mention that H_2 generation through $NaBH_4$ can also been performed through reaction with methanol. In this respect, cobalt bearing materials have also been explored, both in metallic or oxide states, showing a promising behavior towards H_2 generation. For example, in the work of Bekirogullari et al. (2019) [36], nanoparticles of CoB alloy were synthesized over the surface of Vulgaris microalgae, previously functionalized with different acids (HCl, H_3PO_4, acetic). The produced composite was then tested as catalyst for the methanolysis of $NaBH_4$ and H_2 generated volume over time then measured. Hydrogen evolution was carried out at 30°C with 100 mg catalyst and for $NaBH_4$ and NaOH initial concentrations of respectively 2.5 % and 1% (w/w). Best results were achieved for the biomass functionalized with 3 M HCl solution, and a impressive HGR of 13.215 $L.min^{-1}.g^{-1}$ was measured, explained by the highly promoted process kinetics (maximum H_2 reached for a reaction time around 4 min). The favored kinetics reflected on the low global activation energy reported (25.2 $kJ.mol^{-1}$).

During reuse, catalytic activity a measurable catalytic loss was observed for five consecutive reaction cycles, whereas maximum H_2 volume stayed almost the same, but kinetics became progressively slower. In a similar work, Kaia et al. (2019) [37] functionalized with $ZnCl_2$ solution the biomass obtained from spirulina microalgae, which served as a support for CoB nanoparticle synthesis. The obtained composite was next tested for H_2 generation through $NaBH_4$ methanolysis, conducted at 30ºC and 60ºC, with HGR values respectively equal to 9.27 and 36.4 $L.min^{-1}.g^{-1}$. For 100 mg catalyst, best results were achieved with composite containing 30 % (w/w) cobalt, for which maximum H_2 volume (650 mL) was reached for a reaction time around 4 min for an initial solution containing 2.5% (w/w) $NaBH_4$. Authors also studied catalyst reuse for five consecutive reaction cycles at the same reaction conditions and evidenced that maximum H_2 volume stayed almost the same, but kinetics was considerably hindered (reaction time for reaching maximum H_2 production in last cycle almost seven times higher than observed for the first cycle).

Besides cobalt alloys, cobalt oxide containing materials have also been employed as catalysts for borohydride methanolysis. In the work of Prabu and Chiang (2023) [38], for example, Pd-Co_3O_4 hybrid nanostructures were grown over the surface of activated carbon nanosheet produced from coffee. Co-doping with S and N enabled achievement of a composite with very impressive activity at 25ºC with a HGR value of 20.158 $L.g^{-1}.min^{-1}$ and maximum H_2 volume produced in only 25 s reaction time (catalyst mass of 30 mg and 0.4 M NaOH and $NaBH_4$ initial concentrations). As expected, a very low global activation energy was reported (14.52 $kJ.mol^{-1}$).

Therefore, cobalt bearing materials, both in metallic or oxidized state, including those containing the spinel $CoFe_2O_4$ [28 - 38], can be classified as promising materials to be applied as catalysts for H_2 production through $NaBH_4$ hydrolysis. Present research brings an investigation of the use of a new cobalt-iron bearing oxide material as catalyst for hydrogen generation based on the hydrolysis of $NaBH_4$ in aqueous solutions. Although there are some published works covering applications of $CoFe_2O_4$ spinel containing catalysts [35,36], suggesting a promising activity towards H_2 production, present article brings the novelty that the spinel phase is produced through a inovative synthesis procedure, yet not extensively explored in literature, which employs a type of nanocellulose (TCNF) as a reactive template, enabling a satisfactory control of sample morphology and chemical composition, and is based on cobalt and iron simultaneous cation adsorption over the nanofibers surface [39]. Moreover, present research should also contribute with new kinetic data for $NaBH_4$ hydrolysis, which, considering actual energy transition scenario, could be viewed as a viable route for H_2 storage and generation in the future. First, characterization results are presented in order to explore sample morphology and chemical nature and next results from kinetic analysis of H_2 evolution, which was evaluated under the effect of different reaction parameters such as NaOH, $NaBH_4$ initial concentrations, catalyst mass and temperature. Both global reaction order in respect of the borohydride, as well as process activation energy were quantitative evaluated. The obtained catalyst shows a morphology comprising of an aggregate of spherical nanoparticles, and based on the achieve results can be viewed as a potential alternative for other cobalt bearing catalysts already explored in literature.

Methods

Catalyst synthesis

TEMPO-oxidized cellulose nanofibers (TCNF) were obtained, as previously described [40]. Then, 15 mL of nanocellulose aqueous suspension was added to a 100 mL aqueous solution containing Co^{2+} and Fe^{+2} of concentrations respectively equal to 58.21 and 55.75 $g.L^{-1}$, using $Co(NO_3)_2{\cdot}6H_2O$ and $FeSO_4{\cdot}7H_2O$, as cations precursors. After 30 min of contact time, the solid phase was separated through a vacuum filtration and the obtained solid, TCNF fibers with cobalt and iron cations adsorbed on it (TCNF@FeCo), calcinated in a muffle furnace at 500 °C for 2 h.

Hydrogen generation

Hydrogen was performed through use of experimental apparatus depicted in Figure (1). Controlled amounts (± 0.005 g) of sodium hydroxide (NaOH, 99% IsoFar) and sodium borohydride ($NaBH_4$, 97% Nuclear) were dissolved in deionized water, and the homogeneous solution added to a reaction flask, whose temperature was fixed by using of a thermal bath (± 2°C). Then, the desired amount of the catalyst was loaded into the reactor and set under constant stirring. Hydrogen volume generated was then measured as a function of time in a graduate cylinder, with a mean uncertainty of 2%.

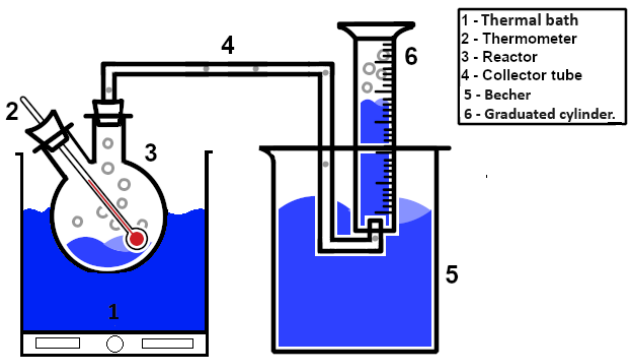

Figure 1. Hydrogen extraction apparatus for catalyzed $NaBH_4$ hydrolysis.

Effect of catalyst mass (12, 25 and 50 mg), NaOH concentration (1.0, 2.5, 5.0 and 10% w/v), $NaBH_4$ concentration (0.5, 1.0, 2.0 and 4.0% w/v) and temperature (10, 25, 40, and 55°C) on the hydrogen production rate were studied. In order to fix temperature in each experiment, a thermal water bath was employed. Kinetic modelling was next performed based on the predicted $NaHB_4$ consumption rate. In order to calculate the time derivative of borohydride concentration as function of time, a second order polynomial fit of $NaBH_4$ of measured data was performed. During kinetic modelling, it was assumed that water was present in excess, and, therefore, its molar amount was considered constant for the calculation of $NaBH_4$ instantaneous concentration. In fact, this assumption is plausible based on the initial molar amounts of borohydride employed, which varied between 0.0025 and 0.02 mol, resulting in a maximum (stoichiometric) water consumption of 0.005 and 0.04 mol, when compared to 1.1 mol of water (20 mL) used in all tests. The obtained polynomial function was then used for the analytical first order derivative calculation, whose negative value represents the desired reaction rate at each time ($-r_a$).

In present article, kinetic modelling was performed through both an empirical model (Equations 2 and 3) and also the Langmuir – Hischelwood (L-H) model (Equations 4) [40], where n designates the reaction order, k represents the kinetic constant, r_a represents the absolute value of the $NaBH_4$ hydrolysis rate at a specified time, $C_{a,0}$ the initial concentration of $NaBH_4$ and K the adsorption equilibrium constant. In the present work, $NaBH_4$ consumption rate was measured in $g.L^{-1}.min^{-1}$ and concentration in $g.L^{-1}$.

$$-r_a = kC_a^n \quad (2)$$

$$\ln(-r_a) = n\, ln(C_a) + lnk \quad (3)$$

$$kt = C_{a,0} - C_a + \frac{ln\left(\frac{C_{a,0}}{C_a}\right)}{K} \quad (4)$$

Regarding the empirical model, a plot of $\ln(-r_a)$ as a function of $ln(C_a)$ enable estimation of global reaction order and kinetic constant, through the linear and angular coefficients, respectively. In case of L-H model a MATLAB function was constructed for simultaneously estimating the values of k and K, which was based on the use of *fminsearch* built-in MATLAB function.

On both cases, process global activation energy (E_a) was calculated from the Arrhenius equation, according to its linearized form (Equation 5), trough evaluation of the angular coefficient of a plot from lnk as a function of $1/T$. In the present work, activation energy is given in J.mol^{-1}, R represents the universal constant gas constant (8.314 J K^{-1} mol^{-1}), and temperature is given in Kelvin.

$$lnk = lnA - \frac{E_a}{RT} \quad (5)$$

In Equation 3, *A* represents the Arrhenius frequency factor, which should be constant as long as no change in the mechanism takes place in temperature range explored, as for both E_a and n.

Recycling tests were carried out three times at 25ºC, 50 mg catalyst mass, and initial concentrations (% w/v) of NaOH and $NaBH_4$ respectively equal 2.5 and 2%. After each reaction cycle, the catalyst was separated from the reaction medium via centrifugation, dried at 80°C overnight, reweighed and finally used for the next reaction cycle. Hydrogen generation rate (HGR) was calculated by dividing the measured rate of H_2 production (L.min^{-1}) by the catalyst mass employed (g).

Sample characterization

X-ray diffraction (XRD) was employed to evaluate sample composition regarding present crystalline phases. Diffraction patterns were obtained employing a Bruker D8 Discover equipped with Ni filter, Lynxeye detector and copper tube operating at 40 mA and 40 kV. Analyses were performed in range between 10 to 95°, 0.02° step and an acquisition time of 15 seconds. Rietveld refinement analysis was performed using TOPAS 5.0 software from Bruker. Sample morphology was first studied through scanning Electron microscopy (SEM) in a JEOL JSM 7100F microscope operating at 2 kV and next through transmission electron microscopy (TEM) in a JEOL JEM 2100F microscope operating at 200 kV.

In order to evaluate sample chemical composition, elemental distribution EDS maps were constructed in STEM mode. To prepare samples for TEM analysis, isopropanol suspensions containing the synthesized oxide particles were drop-casted onto carbon-coated copper grids. Magnetization measurements were performed using a Physical Property Measurement System (PPMS) DynaCool from Quantum Design. Magnetization measurements as a function of the applied magnetic field were conducted at room temperature to analyze the sample's magnetic response, as well as coercive field, saturation magnetization, and remanence magnetization evaluation. Regarding sample preparation for magnetic characterization, powder masses determined using an analytical balance (Mettler Toledo model AB204-S) were carefully wrapped in Teflon tape and positioned in the brass sample holder of the PPMS. Finally, XPS measurements were made using a SPECS system with a *Phoibos 150 hemispherical* analyzer and an aluminum non-monochromatic X-ray gun (1486.6 eV).

A survey and spectra of Fe 2p, Co 2p, C1s and O1s were made and analyzed, removing the Shirley background, deconvolving the peaks using Voight curves. The spectra were corrected using the carbon 1s peak position. In the Cobalt 2p region, the Iron Auger LMM was used in order to perform the desired signal deconvolution.

Results and Discussion

Catalyst characterization

The XRD pattern of the synthesized oxide sample can be observed in Figure 2. According to Rietveld analysis results (Figure A1), it was possible to identify the presence of three crystalline phases, cobalt spinel ferrite ($CoFe_2O_4$, COD CIF file: 1535820) hematite (Fe_2O_3, ICSD, CIF file #82902) and iron III sulfate ($Fe_2(SO_4)_3$, COD CIF file: 9008258), with mass fractions respectively equal to: 74.76 %, 24.98 % and 0.26 % w/w. Figure A1 shows the Rietveld analysis result, whose goodness of fitting (GOF) achieved a value of 1.15, supporting its quantitative level. Mean crystallite sizes were obtained by integral peak breadth-based volume calculation (LVollB), resulting in values of 12 nm and 48 nm for cobalt ferrite and hematite, respectively.

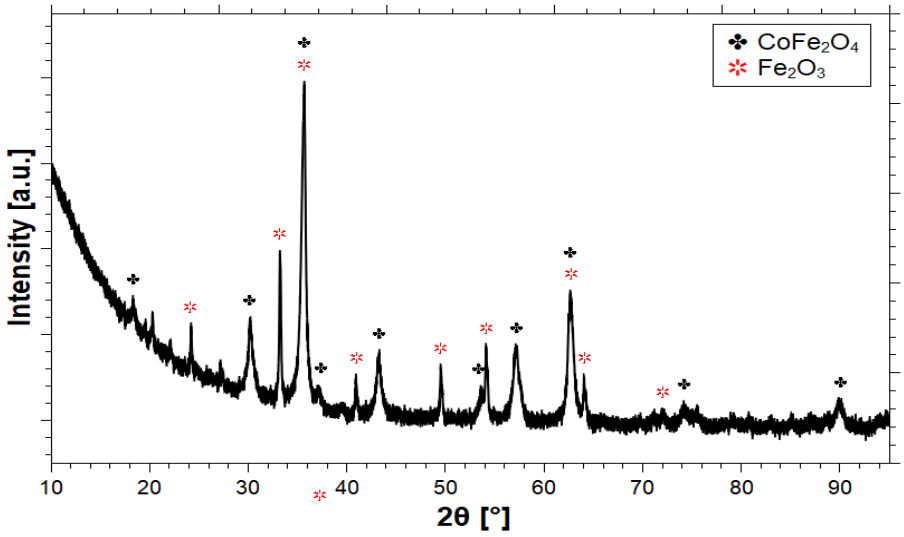

Figure 2. XRD pattern of the sample synthesized in air atmosphere at 500 °C for 2 h.

Formation of spinel structure can be explained by the fact that both Fe^{3+} and Co^{2+} cations, once adsorbed in the TCNF nanofibers, chemically react together with O_2 present in the calcination atmosphere, thereby forming a spinel cubic lattice. On the other hand, hematite (Fe_2O_3) crystals were also produced due to iron excess (free iron cations which do not interact with Co^{2+}) presence over the TCNF fibers. Finally, SO_4^{2-} anions originally present in aqueous media, also adsorbed over TCNF nanofibers, can chemically react with part of the iron cations present, thereby forming iron sulfate, which, according to thermodynamic simulations conducted with software HSC 6.0 should be thermodynamic stable for temperatures in the range between 400 and 800 °C (Figure A2). Simulations have been performed considering an initial amount of 1 mol of sulfate, together with 10 mol of a gaseous mixture containing 8 mol of N_2 and 2 mol of O_2.

Based on data from Figure A2, $Fe_2(SO_4)_3$ can both decompose to Fe_2O_3 or $FeSO_4$, and only after 900 °C no sulfate residue is expected. For the employed calcination temperature (500°C), it is then expected that most part of iron III sulfate formed during sample thermal treatment should be present in the material after calcination step. Therefore, the low mass fraction of iron III sulfate (0.26% w/w) evidenced after Rietveld (Figure A1), together with thermodynamic data of Figure 3 strongly suggest that the amount of sulfate anions (SO_4^{2-}), which adsorbed in TCNF from initial aqueous solution should be of low magnitude, when compared to Fe^{2+} or Co^{3+}, which, in the end, form the major phases identified through XRD analysis, hematite (Fe_2O_3) and cobalt spinel ferrite ($CoFe_2O_4$). Morphology and detailed microstructure of the cobalt-ferrite containing sample can be observed in Figure 3, which depicts TEM data.

Distance between the atom planes in Figure 3c was measured as 0.486 nm, which corresponds to the value of (111) plane of $CoFe_2O_4$. Also, the SAED pattern in Figure 4d was indexed as $CoFe_2O_4$, and the diffraction ring of (111) plane agrees well with the HRTEM image in Figure 3c. These results confirm presence of cobalt ferrite spinel, as evidenced by XRD analysis (Figures 2 and A1). The histogram of the particle size distribution obtained from Figure 3b indicates that the nanoparticles have an average size of 19.0 ± 0.2 nm (Figure A3). Additionally, elemental chemical composition of a group of ferrite nanocrystals was investigated through EDS and corresponding elemental maps and associated STEM image are depicted in Figure 4.

Data clearly reveals that iron, cobalt and oxygen are spatially homogeneously distributed, corroborating the formation of a single spinel phase ($CoFe_2O_4$).

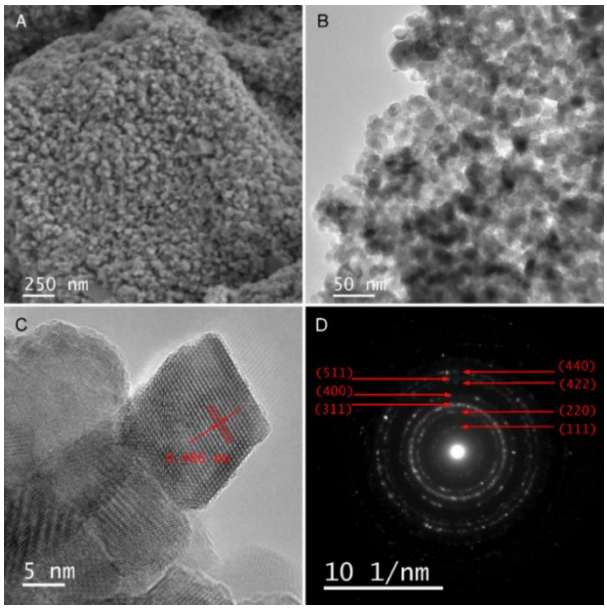

Figure 3. SEM image (A), low magnification TEM image (B), high resolution TEM (HRTEM) image with the spacing between the atomic planes of 0.486 nm, corresponding to the d value of (111) planes of $CoFe_2O_4$ (C), and selected area electron diffraction (SAED) pattern of the sample shown in image B with the structure indexed (D) of the sample calcinated at 500 °C for 2 h in air atmosphere. The index in (D) has been done with the standard powder X-ray diffraction pattern of $CoFe_2O_4$.

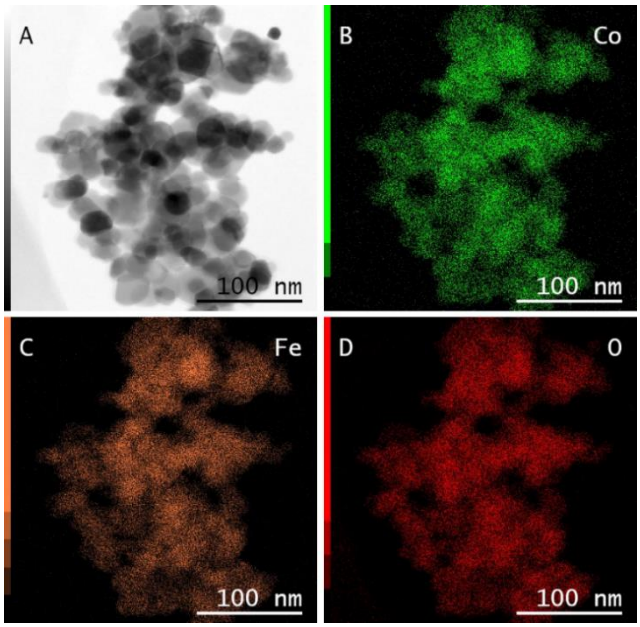

Figure 4. STEM bright field image (A) and associated EDS maps of Co (B), Fe (C), and O (D) of $CoFe_2O_4$.

Magnetization as a function of magnetic field obtained at room temperature (Figure A4) revealed the magnetic characteristics of the studied spinel cobalt – ferrite containing sample. The saturation magnetization (M_s), reaching 37.2 emu g^{-1}, represents the maximum magnetization the material can achieve under the influence of a magnetic field. This value indicates a notable sample magnetic response capacity. On the other hand, the remanence magnetization (M_r), which achieved a value of 15.7 emu g^{-1}, represents the residual magnetization that persists after the removal of the earlier applied external magnetic field. Additionally, the coercive field (H_c) of the sample, measured as 1260 Oe, indicates the material's resistance to demagnetization, i.e., the amount of magnetic field required to completely reverse its magnetization to zero. Also, the observed magnetic behavior (Figure A4) indicates a lower saturation magnetization in comparison with other studies conducted earlier for iron-cobalt spinel crystals [41,42].

This difference can be explained by XRD results presented before (Figures 2 and A1), which revealed the presence of cobalt ferrite spinel, which is magnetic, and hematite, known for its inferior magnetic response due to antiferromagnetic nature [43], therefore contributing for a reduction in M_s. Additionally, TEM analysis (Figure 3) evidenced the presence of nanoparticle agglomeration in the sample. The advent of agglomeration can significantly influence the magnetic properties by promoting magnetic interactions between neighboring particles, thereby leading both to higher values of M_r (residual magnetization) and H_c (coercive field), and also to a hysteresis enhancement, which, for the catalyst mean particle size (19 nm) should not be expected.

XPS analysis

XPS signals associated with catalyst sample as a whole, as well as for the binding energy regions characteristic of iron and cobalt are presented, respectively, in Figures 5, 6 and 7, and, for carbon and oxygen in Figures A5 and A6.

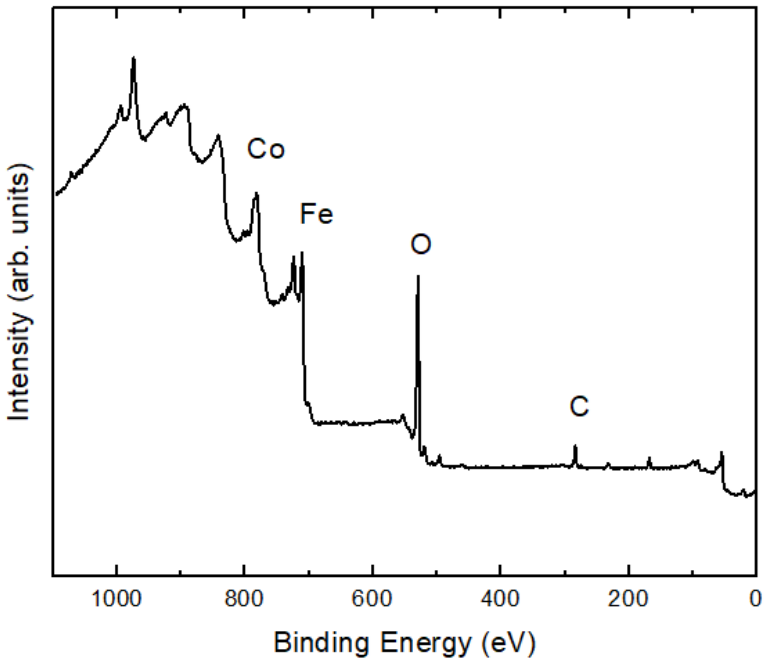

Figure 5. XPS signal for the catalyst sample of interest.

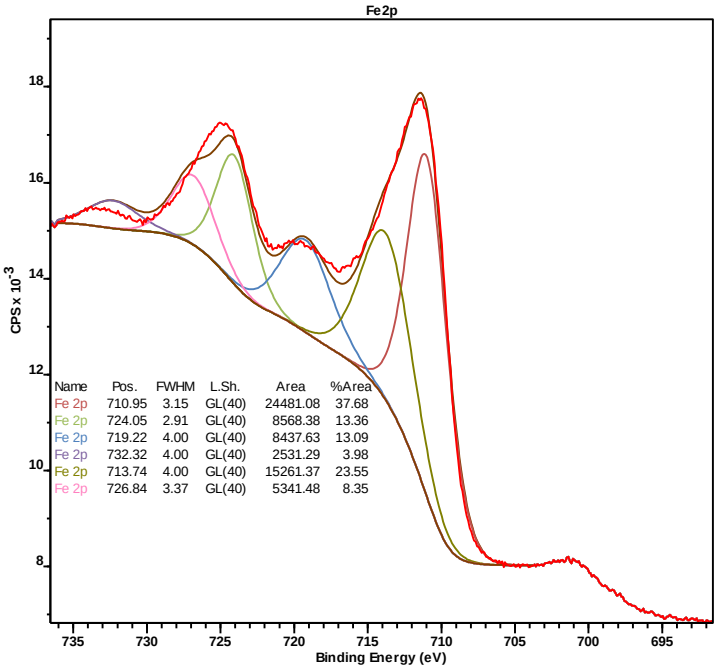

Figure 6. XPS signal for iron binding energy region.

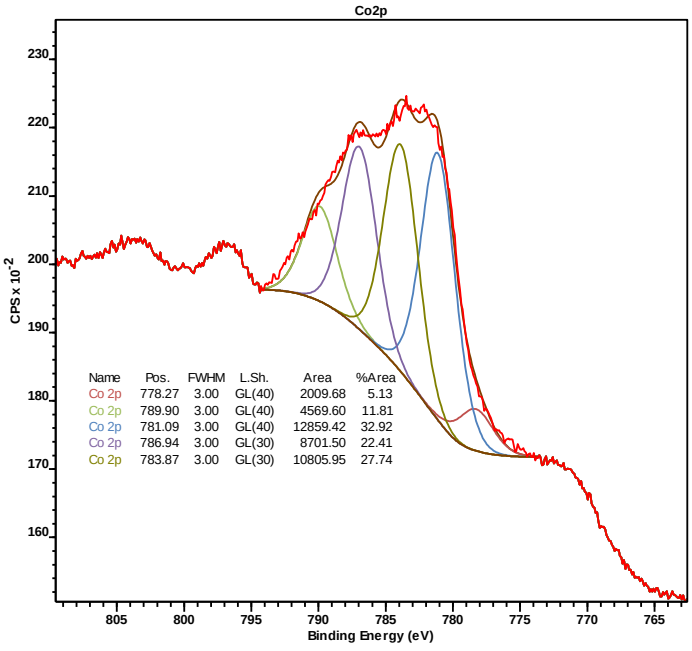

Figure 7. XPS signal for cobalt binding energy region.

Based on the analysis of the above spectra, cobalt to iron ratio in atomic percentage measured by XPS was around 1:3. The cobalt region (Figure 7) presented two different contributions, one related to the octahedral site (780.5 eV) and the other to the tetrahedral site (782.8 eV). The percentage of octahedral sites was approximately 45% and tetrahedral sites was approximately 55%.

Also, in the iron region (Figure 6) we can see two different contributions at 710.8 and 712.9 EV. Regarding the measured spectra, peak at 712.9 could be due to an octahedrally or tetrahedrally coordinated cation with different cation distribution, on the other hand, peak evidenced at 710.8 eV can be associated to the presence of Fe^{+2} [44].

Hydrogen generation

After synthesizing and characterizing the material, our focus shifted to investigating its catalytic behavior, depicted in Figure 8.

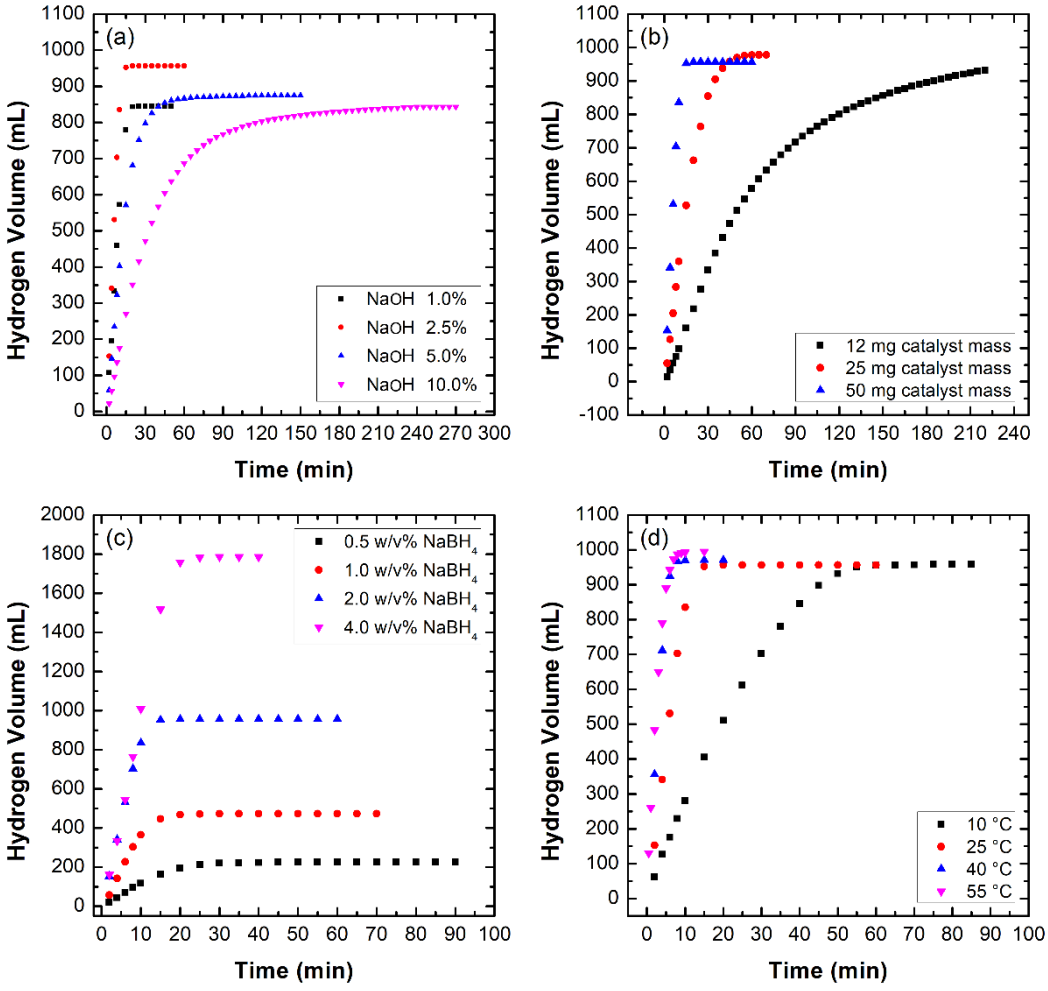

Figure 8. Volume of hydrogen generated as a function of time from catalytic sodium borohydride hydrolysis, varying: NaOH concentration (a), catalyst mass (b), $NaBH_4$ concentration (c) and temperature (d).

Figure 8 shows the obtained data for H_2 generation as a function of time under varying NaOH concentration (Figure 8a), catalyst mass (Figure 8b), $NaBH_4$ concentration (Figure 8c), and temperature (Figure 8d). According to Figure 8, the synthesized cobalt ferrite-containing sample clearly presents a prominent catalytic activity towards hydrogen generation from sodium borohydride aqueous solution in basic media. In order to avoid the $NaBH_4$ self-hydrolysis, NaOH was used as a stabilizing agent, thus, the hydrolysis is controlled by the action of the catalyst [45]. In Table A1, H_2 volume produced after 1 hour for tests conducted without catalyst presence were presented. Under NaOH absence, the amount of H_2 generated at 25°C (123 mL) was almost then times higher in comparison with the amount produced at 55°C for an initial concentration of NaOH equal to 2.5% (10 mL), although much lower than the amount observed under the presence cobalt ferrite catalyst for the same conditions (around 1 L).

Figure 8a presents the kinetic behavior for different NaOH initial concentrations, and shows that when NaOH concentration increases from 1.0 to 2.5 % w/v, maximum H_2 volume increases from around 850 mL (1.0% NaOH) to 956.6 mL (2.5% NaOH), together with slight increase in the observed HGR, with values respectively equal to 1.13 $L.min^{-1}.g^{-1}$ and 1.89 $L.min^{-1}.g^{-1}$. Maximum hydrogen volume obtained has shown to be equal to 956.6 mL, after only 20 min of reaction, using 2.5 % w/v NaOH, 2.0 % w/v $NaBH_4$ and 50 mg of catalyst at 25 °C. This volume is only 8% lower than the one expected for consumption of all $NaBH_4$ present (1040 mL) based on the global reaction stoichiometry (Equation 1). However, higher NaOH concentrations, results in an appreciable reduction of process kinetics. Hydrogen production should be associated with both BH^{-4} complex reduction with concomitant BH_3 formation, but also through BH_3

549 hydrolysis. As pH gets higher, H^+ concentration reduces, making BH_3 formation
550 slower, but, on the other hand, should contribute for the kinetics of water
551 regeneration through $B(OH)_4^-$ oxidation to $B_4O_7^{-2}$, which is kinetically interesting
552 from the BH_3 hydrolysis point of view [30]. Moreover, under high pH, precipitation
553 of low-soluble byproducts could also be present, for example, sodium metaborate
554 and sodium tetrahydroxyborate, thereby blocking access to catalytic sites [46].
555 Hydrogen generation rate is also strongly affected by the catalyst amount
556 (Figure 8b), as demonstrated by the considerable increase in the H_2 generation
557 rate, when catalyst mass increases from 12 mg to 25 mg. A further increase to 50
558 mg does not change maximum H_2 volume appreciably, but contributes
559 considerably to the observed kinetics, as maximum H_2 production is reached after
560 only 15 min for 50 mg catalyst, in comparison to 35 min for 25 mg. Such effect
561 could be explained by the availability of active sites, both for adsorption of
562 reactant species and or involved catalytic reaction steps. The relevance of
563 adsorption for the observed hydrolysis kinetics is supported by the present results
564 achieved with L – H model, which consider adsorption as an important step prior
565 to the chemical transformation over catalyst surface.
566 Next, $NaBH_4$ initial concentration possible effects over H_2 production
567 kinetics was also addressed (Figure 8c). According to the data, there is a visible
568 positive stimulation of reaction kinetics when $NaBH_4$ concentration increased in
569 the interval from 0.5 to 2.0 % w/v. The hydrogen generation rate increased from
570 0.257 to 1.89 $mL.min^{-1}.g_{cat}^{-1}$ when the $NaBH_4$ concentration was varied in this
571 range. As $NaBH_4$ is the source of BH_4^- [30,46], it is understood that an
572 enhancement of its content should have a positive and significant contribution for
573 promoting overall hydrolysis kinetics.

In addition, for the mentioned concentration range, maximum H_2 amount was achieved for 2.0% w/v, which, as said before, is very close to the maximum possible value based on global reaction stoichiometry. A further increase in $NaBH_4$ initial concentration from 2.0 to 4% w/v contributed for the maximum amount of H_2 generated, which for 4% reached a value of 1785 mL, also expressively higher than the one for 2.0% (956.6 mL), but on the other hand, has a negative impact over kinetics, as understood by a comparison of reaction times in order to achieve maximum H_2 production – 13 min (2.0%) and 20 min (4.0%). This could be explained through an increase of solution viscosity, resulting in mass-transfer limitations of BH_4^- species to the active sites available on catalyst surface [47].

Finally, it be observed from Figure 8d that the increase in the temperature, as expected, has a significant effect, enhancing appreciably H_2 generation rate. In this case, as the same initial conditions were employed for all tests (2.5 % w/v NaOH, 2.0 % w/v $NaBH_4$, 50 mg of catalyst), the same maximum H_2 volume is reached, although in shorter reaction times when more thermal energy is available. At 40°C, for example, the maximum amount of H_2 produced (about 956.6 mL) is reached in only approximately 10 min. The calculated specific HGR values (H_2 generation rate per gram of catalyst) as a function of time at different temperatures are presented in Figure 9. As expected based on Figure 8, HGR decreases as time evolves, approaching zero for all three temperatures. Such behavior could be explained, for example, by chemical reaction of the catalyst with the $NaBH_4$, which can act as a reducing agent, resulting in phases containing cobalt and boron in the catalyst surface, also serving as a barrier for contact with the active sites.

This possibility is corroborated by the preliminary results associated with Rietveld analysis for the catalyst after three successive reaction cycles during reuse (Figure A5).

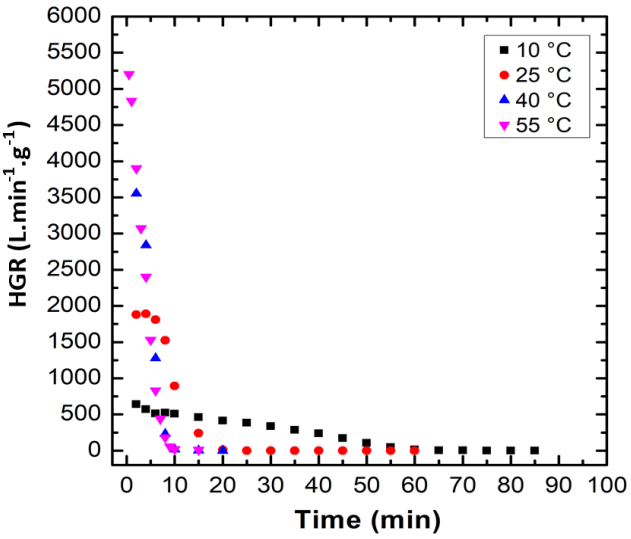

Figure 9. Specific hydrogen generation rate calculated as a function of time for temperature varying between 10 and 55 °C.

Table 1. Comparison of the synthesized catalyst with other reported cobalt-containing catalysts.

Catalyst	HGR (L min^{-1} g_{cat}^{-1})	Temperature (°C)	Reference
$CoFe_2O_4$/oxidized graphene	3.7	22.0	[34]
$CoFe_2O_4$/graphene	8.5	25.0	[33]
$CoFe_2O_4$/Pd	74.8	30.0	[48]
CH_3COOH-kaolin-CoB	1.53	30.0	[30]
Co-Fe complex catalyst	0.69	30.0	[49]
AC (Ni1/Co3/AC)	0.66	30.0	[31]
Co_3O_4 hollow microspheres	5.34	25.0	[50]
$M_{2.5}U_{10}Co_3O_4$-400	2.04	25.0	[51]
CNSs@$Pt_{0.1}Co_{0.9}$	8.94	30.0	[52]
CoO/CaO	0.43	30.0	[53]
Ni-Co-B	2.60	28.0	[54]
$CoFe_2O_4/Fe_2O_3$	1.89	25.0	This work

615 A comparison of activity between present cobalt ferrite spinel containing
616 catalyst and some important $CoFe_2O_4$-based catalysts reported in the literature
617 is given in Table 1. Present maximum specific hydrogen generation rate (HGR),
618 for experiments conducted with 2.0% w/v $NaBH_4$ and 2.5% w/v NaOH at 10, 25,
619 40 and 55 °C, were equal to 0.64, 1.89, 3.55 and 5.20 $L.min^{-1}.g_{cat}^{-1}$, respectively,
620 suggesting a significant and even better catalytic activity when compared with
621 some earlier reported data (see Table 1). It is worthwhile to mention that the
622 synthesized cobalt ferrite catalyst is actually a physical mixture of a spinel phase
623 ($CoFe_2O_4$), hematite (Fe_2O_3), as presented in (Figures 2 and A1). Similar catalytic
624 tests were conducted using a pure hematite sample produced through the same
625 methodology as described before, but with only iron cations (Fe^{3+}) in solution
626 during adsorption step. The amount of H_2 generated (2.0% w/v $NaBH_4$ and 2.5%
627 w/v NaOH, 50mg catalyst), in this case, was insignificant or lower than the
628 detectable limit of the employed experimental apparatus. In the case of iron III
629 sulfate, there is no evidence till present date, that it has any catalytic activity for
630 the process studied in this article. Therefore, in the light of above observations,
631 the authors think that the observed catalytic activity is associated to the presence
632 of the spinel crystals, also, the catalytic active phase in the present context, and
633 could be even enhanced if the spinel phase ($CoFe_2O_4$) could be produced in a
634 state of higher purity.

635 Results obtained during catalyst recycling tests can be appreciated in
636 Figure 10, where the results obtained for a first run (fresh catalyst) at 25 °C were
637 compared with two other successive experiments conducted with the catalyst
638 physically recovered from reaction media. It can be seen that the catalytic activity
639 progressively decreases during cycles.

Figure 11 brings the XRD catalyst sample signal before and after three times being exposed to the same reaction conditions (50 mg catalyst, 2.5% w/v NaOH, 2% w/v $NaBH_4$).

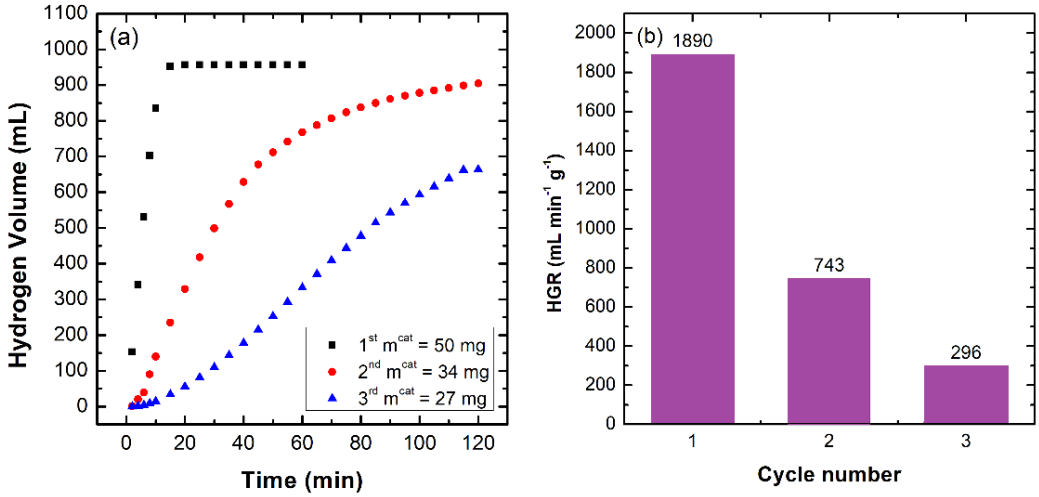

Figure 10. Hydrogen evolution rate during catalyst reuse: a) hydrogen volume as a function of time; b) specific hydrogen generation rate.

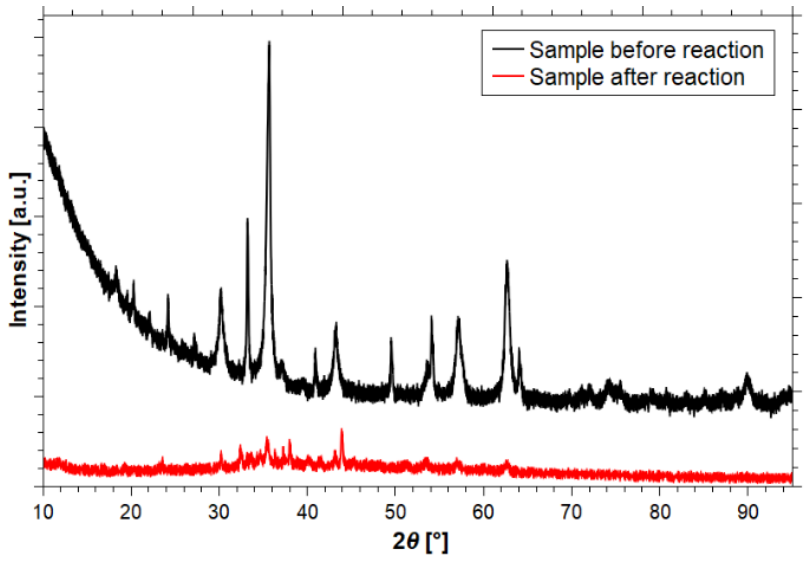

Figure 11. XRD patterns of the sample before and after three successive cycles of hydrogen generation from $NaBH_4$ hydrolysis.

A preliminary Rietveld analysis was performed in order to achieve a first description of the possible crystalline new phases formed and also to quantify the amount of cobalt ferrite after reuse (Figure A5).

667 Results confirmed total absence of hematite after reuse, an also suggests present
668 of a sodium cobalt salt ($CoNa_4O_3$), together with boron and cobalt bearing
669 phases, with chemical formulas, BCo_3 and BCo_3O_5.

670 These findings strongly suggest that a chemical interaction of cobalt ferrite
671 nanocrystals with boron aqueous complexes present in solution took place. This
672 fact, together with reduction of catalyst mass from one reaction cycle to the other
673 could explain the significant loose of catalytic activity during reuse (Figure 10).
674 Reduction of catalyst mass can be explained by strong magnetic character of the
675 sample (Figure 6), mainly associated with $CoFe_2O_4$ particles presence. As a
676 magnetic stirrer was employed, a residual catalyst amount stayed adhered to its
677 surface during each reaction batch, also explaining why catalyst mass was not
678 constant between consecutive reaction cycles. Therefore, authors believe that
679 through use of a mechanical stirrer instead of the magnetic one, catalytic activity
680 could be even further enhanced. Catalyst sample strong magnetic character can
681 be clearly depicted in Figure A5, which illustrates the significant attraction of
682 cobalt ferrite containing particles to the external applied magnetic field.

683 **Kinetic modelling**

684 Based on kinetic data obtained at 25ºC for 50mg catalyst, and
685 concentrations (% w/v) of NaOH and $NaBH_4$ respectively equal to 2.5% and 2%
686 (Figure 7), a preliminary kinetic model for the global process was constructed.
687 Based on stoichiometry of the global process involved (Equation 1), volume of H_2
688 at each time was used in order to calculate the amount of $NaBH_4$ present, and,
689 after a second order polynomial fit, $NaBH_4$ consumption rate was computed,
690 whose variation with time was correlated based on the linear model defined by
691 Eq. (3).

Both the polynomial fit and subsequent linear regression resulted in a quantitative description of the experimental data (Figure 12). Reaction global order was equal to 0.584 and kinetic constant equal to 0.437, with a very good R^2 value of 0.999.

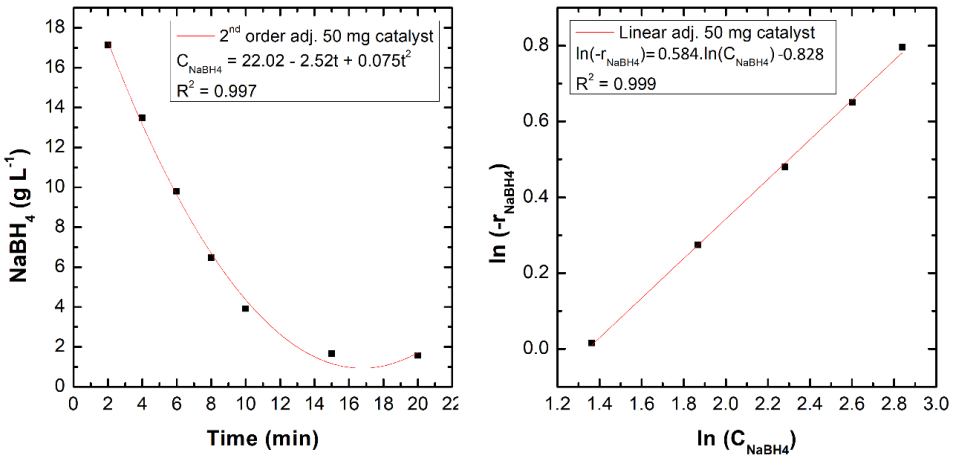

Figure 12. Polynomial fit and linear plot for reaction data at 25ºC, 2% w/v $NaBH_4$, 2.5 % w/v NaOH, 50 mg catalyst.

Regarding L - H model, both reaction constant (*k*) and adsorption (*K*) constant were simultaneously estimated against experimental data, according to Equation 4, and, according to Figure (13), a very good agreement with experimental data was also observed (R^2 = 0.997). In Figure 13, "vkt" denotes the product of reaction constant against time (kt).

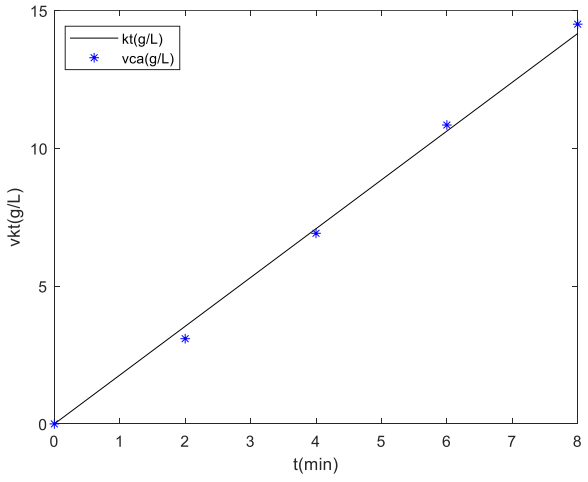

Figure 13. Fitting to LH model for reaction data at 25ºC for 2% w/v $NaBH_4$, 2.5 % w/v NaOH, 50 mg catalyst.

Employing the estimated kinetic parameters for computing $NaBH_4$ concentration as a function of time, with both models for the time interval considered during parameter fitting, plots of Figure 14.

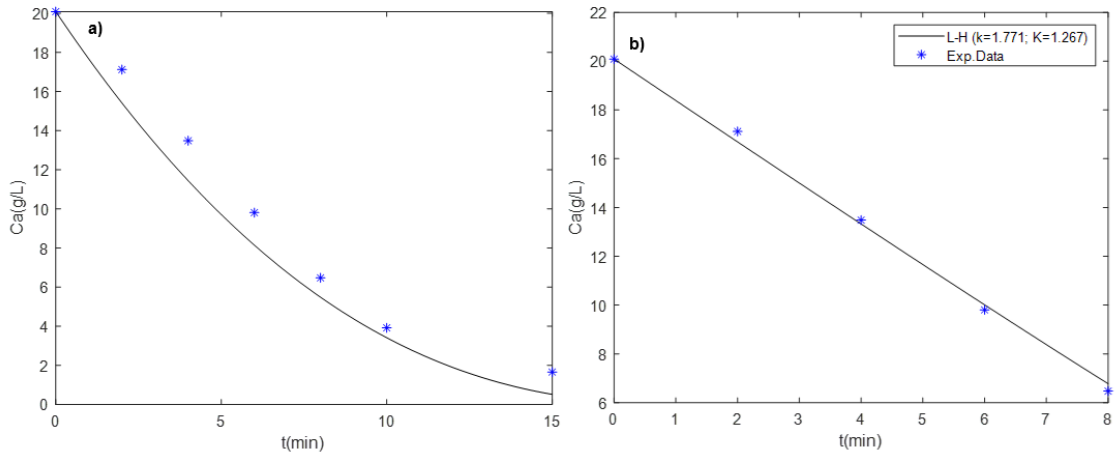

Figure 14. Experimental and calculated $NaBH_4$ concentration with empirical model at 25ºC (2% w/v $NaBH_4$, 2.5 % w/v NaOH, 50 mg catalyst: a) empirical model; b) L-H model.

Clearly, regarding the empirical model, there are some measurable differences between experimental and calculated value, with a mean relative deviation (absolute deviation of calculated and experimental value divided by the experimental value) of 19.9% for a time interval between 0 and 15 min, indicating that the proposed empirical model is not able to describe the complexity of the reaction system under study, even considering data in the region covered during estimation procedure. On the other hand, for the L-H model the same is not truth, and a mean relative deviation of 2.1% was observed.

According to literature [30,43], indeed, reaction mechanism should involve, besides participation of different boron aqueous complexes, for example, BH_4^- or $B(OH)_4^-$, multiple reaction steps, some of them including direct participation of water molecules. Moreover, the reaction system can also be affected by mass transfer from species in solution to the catalytic active sites. In this context, it should be noted that Langmuir – Hischelwood model [40] assumes that both

adsorption and chemical reaction contributes for the observed reaction rate, and indeed, was the model that best fitted the experimental data used for k and K estimation.

Regarding H_2 production conducted with 50 mg catalyst, 2.0 % w/v $NaBH_4$, and 2.5 % w/v NaOH, temperature was varied and kinetic data for 10°C and 55°C were obtained and were treated in the same way as data at 25°C. Through an Arrhenius (Figure 15), global activation energies have been determined: 42.2 ± 5.8 kJ/mol (L - H), 38.4 ± 5.3 K (empirical model). In both cases, R^2 values very close to unity were observed, being equal to 0.998 and 0.882 for L – H and empirical model respectively.

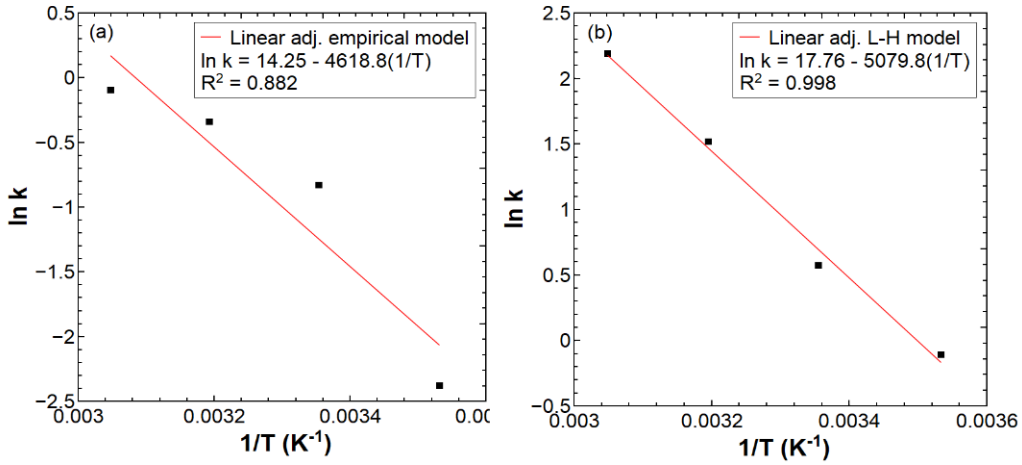

Figure 15. Arrhenius plot for global activation (E_a) evaluation: a) Empirical model; b) Langmuir – Hischelwood.

It should be noted that under estimated precision these values are consistent with each other and also with earlier data for other cobalt catalysts already reported in literature (see Table 2). Values for estimated parameters and R^2 coefficients can be found in Tables A2 and A3. The low E_a values estimated with present data for both models could suggest that either diffusion should have a strong influence for kinetics considering the experimental setup employed [55], or that the reaction path achievable through $CoFe_2O_4$ crystals presence is really effective in reducing

753 the activation energy needs for H_2 molecules formation over the catalyst surface,
754 topics that could be handled in future publications.

755 **Table 2.** Global activation energy for H_2 extraction from $NaBH_4$ hydrolysis for different cobalt-
756 containing catalysts.

Catalyst	Activation Energy (kJ mol $^{-1}$)	Reference
$CoFe_2O_4$/oxidized graphene	31.4	[34]
$CoFe_2O_4$/Pd	63.1	[48]
CoBFe	74.0	[23]
CH_3COOH-kaolin-CoB	49.4	[30]
AC (Ni1/Co3/AC)	50.0	[31]
Co_3O_4 hollow microspheres	42.5	[50]
CNSs@$Pt_{0.1}Co_{0.9}$	38.0	[52]
CoO/CaO	16.7	[53]
Plasma treated Co-B-P	49.1	[28]
Ni-Co-B	62.0	[54]
$CoFe_2O_4/Fe_2O_3$	38.4 ± 5.3	This work (empirical model)
$CoFe_2O_4/Fe_2O_3$	42.2 ± 5.8	This work (L-H model)

757

758 ## Conclusions

759 Present study focused in the synthesis, characterization and catalytic
760 activity towards H_2 extraction from $NaBH_4$ aqueous solutions of a cobalt ferrite
761 containing sample produced synthesized through a novel and simple chemical
762 route, based on the use of nanocellulose (TCNF) fibers as a reactive template
763 during oxide formation. Rietveld analysis applied to the XRD signal of the
764 produced oxide material revealed presence of a cobalt spinel phase ($CoFe_2O_4$),
765 hematite (Fe_2O_3) and residual iron sulfate ($Fe_2(SO_4)_3$), with mass fractions
766 respectively equal to 74.26%, 24.98% and 0.76% w/w.

Characterization through TEM revealed presence of agglomerates of spheroidal shape particles with a mean diameter of 19.6 nm. Also, EDS maps confirmed that cobalt, iron and oxygen should be present in the same phase, exhibiting a uniform spatial distribution. Moreover, the synthesized sample also showed an impressive magnetic behavior, achieving a specific saturation magnetization of 37.2 $emu.g^{-1}$ for a magnetic field of 30 kOe. Appreciable magnetic hysteresis, with remanence magnetization of 15.7 $emu.g^{-1}$ and a coercive field of 1.26 kOe were evidenced, and contrast, in a first glance, with the low mean particle size (19.6 nm) quantified through TEM analysis. This evidence could be explained by formation of particle agglomerates, which were also evident during characterization through TEM.

Contact of $CoFe_2O_4$ with $NaBH_4$ under the presence of NaOH in aqueous solutions showed a remarkable hydrogen generation potential, achieving an impressive maximum volume of 1785 mL for 4.0 % w/v, $NaBH_4$, 2.5% w/v NaOH and 50 mg catalyst, which was very close to the maximum allowed through stoichiometric considerations (2086 mL) and was achieved after only 15 min reaction time. Also, for 50 mg catalyst and initial concentrations of NaOH and $NaBH_4$ respectively equal to 2.5% and 2.0% (w/v) a specific hydrogen generation rate of 2.84 L min^{-1} g_{cat}^{-1} was evidenced at 40 °C, which is competitive with many cobalt based catalysts already reported in literature. For the same catalyst, NaOH and $NaBH_4$ initial conditions, process global activation energy was evaluated in the range between 10 and 55ºC for both the empirical (38.4 ± 5.3 kJ/mol) and L-H (42.2 ± 5.8 kJ/mol) models, and obtained values are in accordance with earlier values reported for the same reaction process and other cobalt containing oxide catalysts. It is worth mentioning that a competitive behavior was observed, which is remarkable, because $CoFe_2O_4$ containing materials already reported in

literature are usually obtained through much more complex and expensive synthesis routes, such as the ones applied for either graphene – $CoFe_2O_4$ [32] or graphene oxide – $CoFe_2O_4$ composites [33].

Reuse tests conducted at 25ºC for NaOH and $NaBH_4$ initial concentrations of 2.5% and 2.0% w/w indicated an appreciable reduction in catalytic activity of 84%, considering the first and third reaction cycles. This could be both attributed to possible chemical interactions of $CoFe_2O_4$ crystals with borohydride ions available in solution, as suggested by Rietveld analysis of catalyst XRD data after reuse, but also to an appreciable reduction of catalyst mass from the first run (50 mg) to the third (27 mg) due to losses resulting from catalyst particles adhered to magnetic stirrer employed.

Acknowledgements

Author Lucas Tonetti would like to thank CNPQ for a scholarship grant (141612/2020-7) and Rogério Siqueira FAPERJ for financial support to present research project development (E26/211.661/2021).

References

[1] Hao Y, Chen P. Do renewable energy consumption and green innovation help to curb CO2 emissions? Evidence from E7 countries. Environmental Science and Pollution Research 2023;30:21115–31. https://doi.org/10.1007/s11356-022-23723-0.

[2] Sarker AK, Azad AK, Rasul MG, Doppalapudi AT. Prospect of Green Hydrogen Generation from Hybrid Renewable Energy Sources: A Review. Energies (Basel) 2023;16. https://doi.org/10.3390/en16031556.

[3] Michael E. Mann. The new climate war: the fight to take back our planet. vol. 1. 1st ed. New York: PublicAffairs; 2021.

[4] Mehrjerdi H. Modeling and optimization of an island water-energy nexus powered by a hybrid solar-wind renewable system. Energy 2020;197. https://doi.org/10.1016/j.energy.2020.117217.

[5] Chen L, Qi Z, Zhang S, Su J, Somorjai GA. Catalytic hydrogen production from methane: A review on recent progress and prospect. Catalysts 2020;10. https://doi.org/10.3390/catal10080858.

[6] Lee JE, Jeon KJ, Show PL, Lee IH, Jung SC, Choi YJ, et al. Mini review on H2 production from electrochemical water splitting according to special nanostructured morphology of electrocatalysts. Fuel 2022;308. https://doi.org/10.1016/j.fuel.2021.122048.

[7] Momirlan M, Veziroglu TN. The properties of hydrogen as fuel tomorrow in sustainable energy system for a cleaner planet. Int J Hydrogen Energy 2005;30:795–802. https://doi.org/10.1016/j.ijhydene.2004.10.011.

[8] Santos DMF, Sequeira CAC. Sodium borohydride as a fuel for the future. Renewable and Sustainable Energy Reviews 2011;15:3980–4001. https://doi.org/10.1016/j.rser.2011.07.018.

[9] Nazir H, Muthuswamy N, Louis C, Jose S, Prakash J, Buan ME, et al. Is the H2 economy realizable in the foreseeable future? Part II: H2 storage, transportation, and distribution. Int J Hydrogen Energy 2020;45:20693–708. https://doi.org/10.1016/j.ijhydene.2020.05.241.

[10] Boran A, Erkan S, Ozkar S, Eroglu I. Kinetics of hydrogen generation from hydrolysis of sodium borohydride on Pt/C catalyst in a flow reactor. Int J Energy Res 2013;37:443–8. https://doi.org/10.1002/er.3007.

[11] Retnamma R, Novais AQ, Rangel CM. Kinetics of hydrolysis of sodium borohydride for hydrogen production in fuel cell applications: A review. Int J Hydrogen Energy 2011;36:9772–90. https://doi.org/10.1016/j.ijhydene.2011.04.223.

[12] Abdelhamid HN. A review on hydrogen generation from the hydrolysis of sodium borohydride. Int J Hydrogen Energy 2021;46:726–65. https://doi.org/10.1016/j.ijhydene.2020.09.186.

[13] Demirci UB, Akdim O, Andrieux J, Hannauer J, Chamoun R, Miele P. Sodium borohydride hydrolysis as hydrogen generator: Issues, state of the art and applicability upstream froma fuel cell. Fuel Cells 2010;10:335–50. https://doi.org/10.1002/fuce.200800171.

[14] Dai P, Zhao X, Xu D, Wang C, Tao X, Liu X, et al. Preparation, characterization, and properties of Pt/Al2O3/cordierite monolith catalyst for hydrogen generation from hydrolysis of sodium borohydride in a flow reactor. Int J Hydrogen Energy 2019;44:28463–70. https://doi.org/10.1016/j.ijhydene.2019.02.013.

[15] Huff C, Dushatinski T, Abdel-Fattah TM. Gold nanoparticle/multi-walled carbon nanotube composite as novel catalyst for hydrogen evolution reactions. Int J Hydrogen Energy 2017;42:18985–90. https://doi.org/10.1016/j.ijhydene.2017.05.226.

[16] Al-Thabaiti SA, Khan Z, Malik MA. Bimetallic Ag-Ni nanoparticles as an effective catalyst for hydrogen generation from hydrolysis of sodium borohydride. Int J Hydrogen Energy 2019;44:16452–66. https://doi.org/10.1016/j.ijhydene.2019.04.240.

[17] Liu Z, Guo B, Chan SH, Tang EH, Hong L. Pt and Ru dispersed on LiCoO2 for hydrogen generation from sodium borohydride solutions. J Power Sources 2008;176:306–11. https://doi.org/10.1016/j.jpowsour.2007.09.114.

[18] Patel N, Patton B, Zanchetta C, Fernandes R, Guella G, Kale A, et al. Pd-C powder and thin film catalysts for hydrogen production by hydrolysis of sodium borohydride. Int J Hydrogen Energy 2008;33:287–92. https://doi.org/10.1016/j.ijhydene.2007.07.018.

[19] Hung TF, Kuo HC, Tsai CW, Chen HM, Liu RS, Weng BJ, et al. An alternative cobalt oxide-supported platinum catalyst for efficient hydrolysis of sodium borohydride. J Mater Chem 2011;21:11754–9. https://doi.org/10.1039/c1jm11720c.

[20] Demirci UB, Akdim O, Hannauer J, Chamoun R, Miele P. Cobalt, a reactive metal in releasing hydrogen from sodium borohydride by hydrolysis: A short review and a research perspective. Sci China Chem, vol. 53, Science in China Press; 2010, p. 1870–9. https://doi.org/10.1007/s11426-010-4081-1.

[21] H. I. Schlesinger, Herbert C. Brown, A. . Finholt, James R. Gilbreath, Henry R. Hoekstra, Earl K. Hyde. Sodium borohydride, its hydrolysis and its use as a reducing agent and in the generation of hydrogen. J Am Chem Soc 1953;75:215–9. https://doi.org/10.1021/ja01097a057.

[22] Liu BH, Li Q. A highly active Co-B catalyst for hydrogen generation from sodium borohydride hydrolysis. Int J Hydrogen Energy 2008;33:7385–91. https://doi.org/10.1016/j.ijhydene.2008.09.055.

[23] Balčiūnaitė A, Sukackienė Z, Antanavičiūtė K, Vaičiūnienė J, Naujokaitis A, Tamašauskaitė-Tamašiūnaitė L, et al. Investigation of hydrogen generation from sodium borohydride using different cobalt catalysts. Int J Hydrogen Energy 2021;46:1989–96. https://doi.org/10.1016/j.ijhydene.2020.10.047.

[24] Demirci UB, Miele P. Reaction mechanisms of the hydrolysis of sodium borohydride: A discussion focusing on cobalt-based catalysts. Comptes Rendus Chimie 2014;17:707–16. https://doi.org/10.1016/j.crci.2014.01.012.

[25] Muir SS, Yao X. Progress in sodium borohydride as a hydrogen storage material: Development of hydrolysis catalysts and reaction systems. Int J Hydrogen Energy 2011;36:5983–97. https://doi.org/10.1016/j.ijhydene.2011.02.032.

[26] da Silva M V., Fajardo H V., Rodrigues TS, e Silva FA, Bergamaschi VS, Dias A, et al. Synthesis of NiMoO4 ceramics by proteic sol-gel method and investigation of their catalytic properties in hydrogen production. Mater Chem Phys 2021;262. https://doi.org/10.1016/j.matchemphys.2021.124301.

[27] Demirci UB, Miele P. Cobalt-based catalysts for the hydrolysis of NaBH4 and NH 3BH3. Physical Chemistry Chemical Physics 2014;16:6872–85. https://doi.org/10.1039/c4cp00250d.

[28] Şahin Ö, Karakaş DE, Kaya M, Saka C. The effects of plasma treatment on electrochemical activity of Co–B–P catalyst for hydrogen production by hydrolysis of NaBH4. Journal of the Energy Institute 2017;90:466–75. https://doi.org/10.1016/j.joei.2016.03.003.

[29] Hani Nasser Abdelhamid. Solid Acid Zirconium Oxo Sulfate/Carbon-Derived UiO-66 for Hydrogen Production. Energy and Fuels 2021;35:10322–6. https://doi.org/10.1021/acs.energyfuels.1c00516.

[30] Saka C, Eygi MS, Balbay A. Cobalt loaded organic acid modified kaolin clay for the enhanced catalytic activity of hydrogen release via hydrolysis of sodium borohydride. Int J Hydrogen Energy 2021;46:3876–86. https://doi.org/10.1016/j.ijhydene.2020.10.201.

[31] Didehban A, Zabihi M, Shahrouzi JR. Experimental studies on the catalytic behavior of alloy and core-shell supported Co-Ni bimetallic nano-catalysts for hydrogen generation by hydrolysis of sodium borohydride. Int J Hydrogen Energy 2018;43:20645–60. https://doi.org/10.1016/j.ijhydene.2018.09.127.

[32] Durano MM, Tamboli AH, Kim H. Cobalt oxide synthesized using urea precipitation method as catalyst for the hydrolysis of sodium borohydride. Colloids Surf A Physicochem Eng Asp 2017;520:355–60. https://doi.org/10.1016/j.colsurfa.2017.02.005.

[33] Jafarzadeh H, Karaman C, Güngör A, Karaman O, Show PL, Sami P, et al. Hydrogen production via sodium borohydride hydrolysis catalyzed by cobalt ferrite anchored nitrogen-and sulfur co-doped graphene hybrid nanocatalyst: Artificial neural network modeling approach. Chemical Engineering Research and Design 2022;183:557–66. https://doi.org/10.1016/j.cherd.2022.05.038.

[34] Karami M, Fathirad F. Cobalt ferrite nanoparticles anchored on reduced graphene oxide nanoribbons (0D/1D CoFe2O4/rGONRs) as an efficient catalyst for hydrogen generation via NaBH4 hydrolysis. Inorg Chem Commun 2023;150. https://doi.org/10.1016/j.inoche.2023.110552.

[35] Deonikar VG, Rathod P V., Pornea AM, Puguan JMC, Park K, Kim H. Hydrogen generation from catalytic hydrolysis of sodium borohydride by a Cu and Mo promoted Co catalyst. Journal of Industrial and Engineering Chemistry 2020;86:167–77. https://doi.org/10.1016/j.jiec.2020.02.024.

[36] Bekiroğullari M, Kaya M, Saka C. Highly efficient Co-B catalysts with Chlorella Vulgaris microalgal strain modified using hydrochloric acid as a new support material for hydrogen production from methanolysis of sodium borohydride. Int J Hydrogen Energy 2019;44:7262–75. https://doi.org/10.1016/j.ijhydene.2019.01.246.

[37] Kaya M, Bekiroğullari M, Saka C. Highly efficient CoB catalyst using a support material based on Spirulina microalgal strain treated with ZnCl2 for hydrogen generation via sodium borohydride methanolysis. Int J Energy Res 2019;43:4243–52. https://doi.org/10.1002/er.4548.

[38] Prabu S, Chiang KY. Synergistic effect of Pd-Co3O4 nanoparticles supported on coffee-derived sulfur, nitrogen-codoped hierarchical porous carbon for efficient methanolysis of NaBH4. J Alloys Compd 2023;938. https://doi.org/10.1016/j.jallcom.2022.168548.

[39] Teixeira LT, de Lima SLS, Rosado TF, Liu L, Vitorino HA, dos Santos CC, et al. Sustainable Cellulose Nanofibers-Mediated Synthesis of Uniform Spinel Zn-Ferrites Nanocorals for High Performances in Supercapacitors. Int J Mol Sci 2023;24:9169. https://doi.org/10.3390/ijms24119169.

[40] Andrieux J, Demirci UB, Miele P. Langmuir-Hinshelwood kinetic model to capture the cobalt nanoparticles-catalyzed hydrolysis of sodium borohydride over a wide temperature range. Catal Today 2011;170:13–9. https://doi.org/10.1016/j.cattod.2011.01.019.

[41] Goh SC, Chia CH, Zakaria S, Yusoff M, Haw CY, Ahmadi S, et al. Hydrothermal preparation of high saturation magnetization and coercivity cobalt ferrite nanocrystals without subsequent calcination. Mater Chem Phys 2010;120:31–5. https://doi.org/10.1016/j.matchemphys.2009.10.016.

[42] Baldi G, Bonacchi D, Innocenti C, Lorenzi G, Sangregorio C. Cobalt ferrite nanoparticles: The control of the particle size and surface state and their effects on magnetic properties. J Magn Magn Mater 2007;311:10–6. https://doi.org/10.1016/j.jmmm.2006.11.157.

[43] Winsett J, Moilanen A, Paudel K, Kamali S, Ding K, Cribb W, et al. Quantitative determination of magnetite and maghemite in iron oxide nanoparticles using Mössbauer spectroscopy. SN Appl Sci 2019;1. https://doi.org/10.1007/s42452-019-1699-2.

[44] Fantauzzi M, Secci F, Sanna Angotzi M, Passiu C, Cannas C, Rossi A. Nanostructured spinel cobalt ferrites: Fe and Co chemical state, cation distribution and size effects by X-ray photoelectron spectroscopy. RSC Adv 2019;9:19171–9. https://doi.org/10.1039/c9ra03488a.

[45] Li H, Hu X, Wang L, Shi L, Isimjan TT, Yang X. Kinetically promoted hydrogen generation by Ru nanoparticles decorated CoB2O4 on mesoporous carbon spheres with rich oxygen vacancies for NaBH4 hydrolysis. Chemical Engineering Journal 2024;481. https://doi.org/10.1016/j.cej.2024.148547.

[46] Lin F, Zhang A, Zhang J, Yang L, Zhang F, Li R, et al. Hydrogen generation from sodium borohydride hydrolysis promoted by MOF-derived carbon supported cobalt catalysts. Colloids Surf A Physicochem Eng Asp 2021;626. https://doi.org/10.1016/j.colsurfa.2021.127033.

[47] Şahin Ö, Kılınç D, Saka C. Bimetallic Co–Ni based complex catalyst for hydrogen production by catalytic hydrolysis of sodium borohydride with an alternative approach. Journal of the Energy Institute 2016;89:617–26. https://doi.org/10.1016/j.joei.2015.05.007.

[48] Wang Y, Liu X. Catalytic Hydrolysis of Sodium Borohydride for Hydrogen Production Using Magnetic Recyclable CoFe2O4-Modified Transition-Metal Nanoparticles. ACS Appl Nano Mater 2021;4:11312–20. https://doi.org/10.1021/acsanm.1c03067.

[49] Şahin Ö, Kilinç D, Saka C. Hydrogen Production by Catalytic Hydrolysis of Sodium Borohydride with a Bimetallic Solid-State Co-Fe Complex Catalyst. Separation Science and Technology (Philadelphia) 2015;50:2051–9. https://doi.org/10.1080/01496395.2015.1016040.

[50] Wang Q, Wei L, Ma M, Liu H. Hydrogen generation from the hydrolysis of sodium borohydride using Co3O4 hollow microspheres as high-efficient catalyst precursor synthesized by facile bio-template method. Energy Sources, Part A: Recovery, Utilization and Environmental Effects 2020. https://doi.org/10.1080/15567036.2020.1805046.

[51] Mengesha DN, Baye AF, Kim H. Modulating effect of urea/melamine on Co2+/Co3+ ratio of Co3O4 microplates for rapid hydrogen generation via NaBH4 hydrolysis. Int J Hydrogen Energy 2024;57:856–68. https://doi.org/10.1016/j.ijhydene.2024.01.085.

[52] Zhang H, Zhang L, Rodríguez-Pérez IA, Miao W, Chen K, Wang W, et al. Carbon nanospheres supported bimetallic Pt-Co as an efficient catalyst for NaBH4 hydrolysis. Appl Surf Sci 2021;540. https://doi.org/10.1016/j.apsusc.2020.148296.

[53] Altınsoy M, Ceyhan AA. Synthesis of cobalt-doped catalyst for NaBH4 hydrolysis using eggshell biowaste. Int J Hydrogen Energy 2023;48:28018–33. https://doi.org/10.1016/j.ijhydene.2023.04.047.

[54] Ingersoll JC, Mani N, Thenmozhiyal JC, Muthaiah A. Catalytic hydrolysis of sodium borohydride by a novel nickel-cobalt-boride catalyst. J Power Sources 2007;173:450 -7. https://doi.org/10.1016/j.jpowsour.2007.04.040.

[55] H. Scott Fogler *Elements of Chemical Reaction Engineering*; 5º Edition.; Pearson Education, Inc.: Michigan, 2016.

Appendix

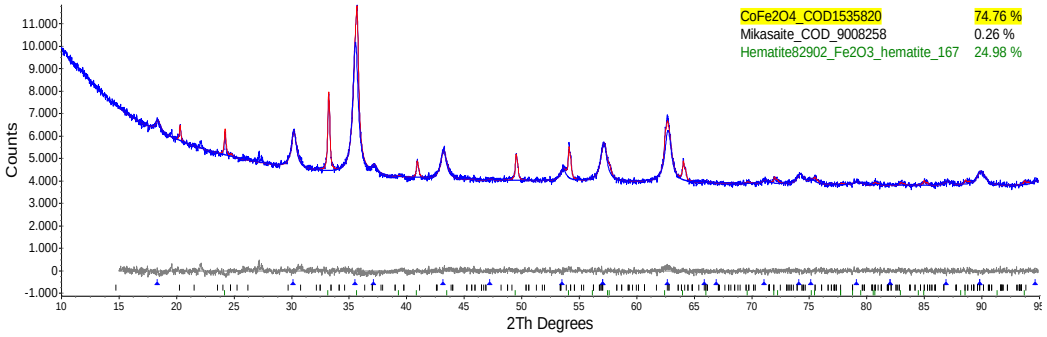

Figure A1. Rietveld Refinement for cobalt ferrite catalyst sample.

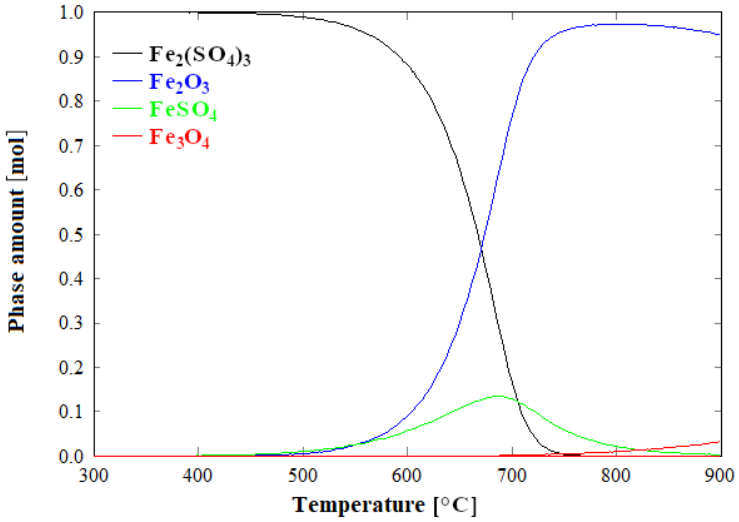

Figure A2. Speciation diagram for iron III sulfate thermal decomposition under air atmosphere.

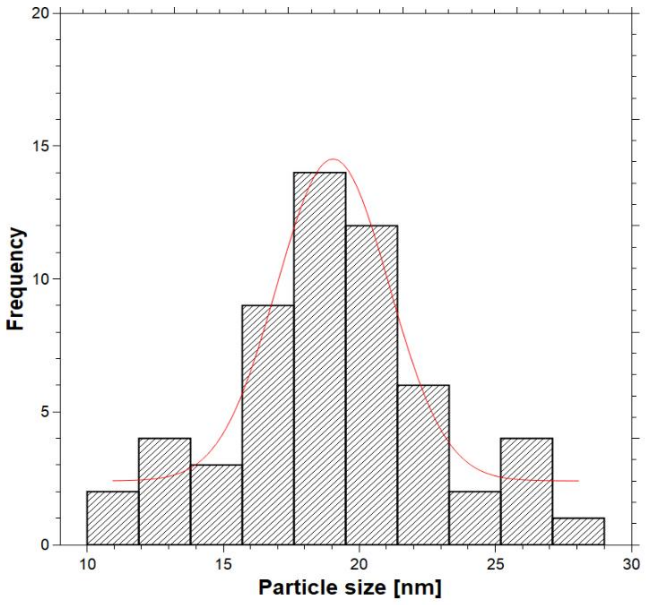

Figure A3. Particle size distribution based on TEM analysis.

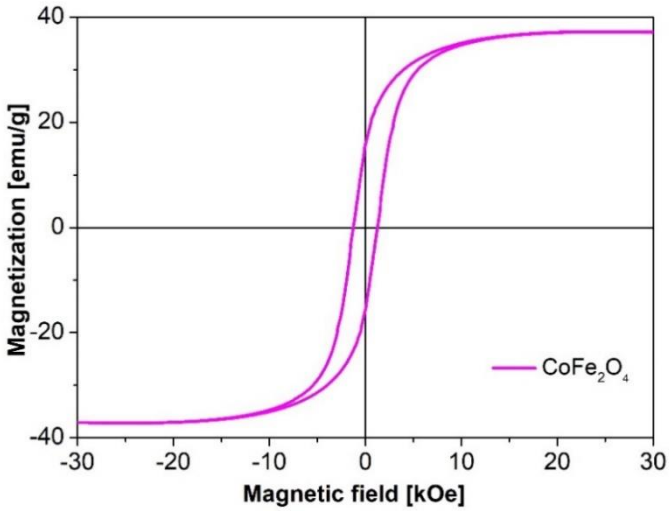

Figure A4. Magnetization as a function of magnetic field at room temperature of $CoFe_2O_4$ ferrite.

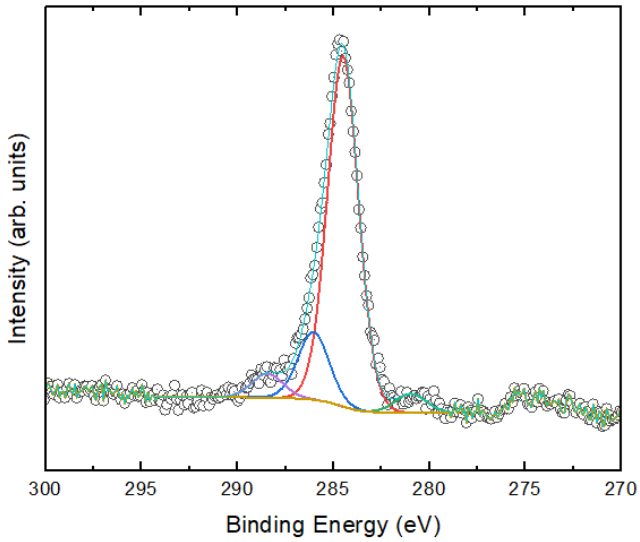

Figure A5. XPS signal for carbon binding energy range.

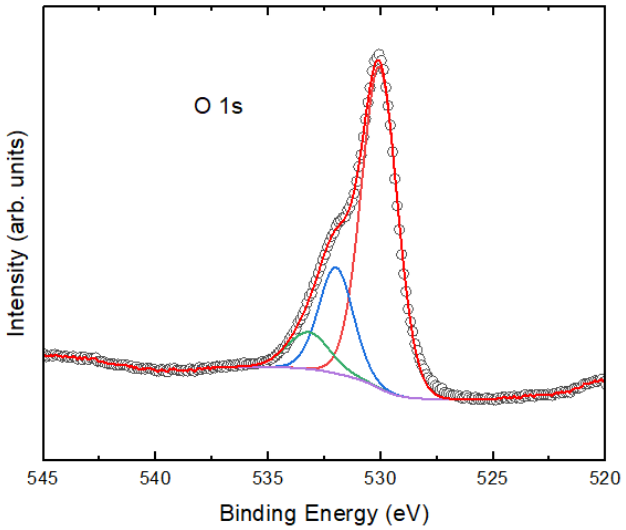

Figure A6. XPS signal for oxygen binding energy range.

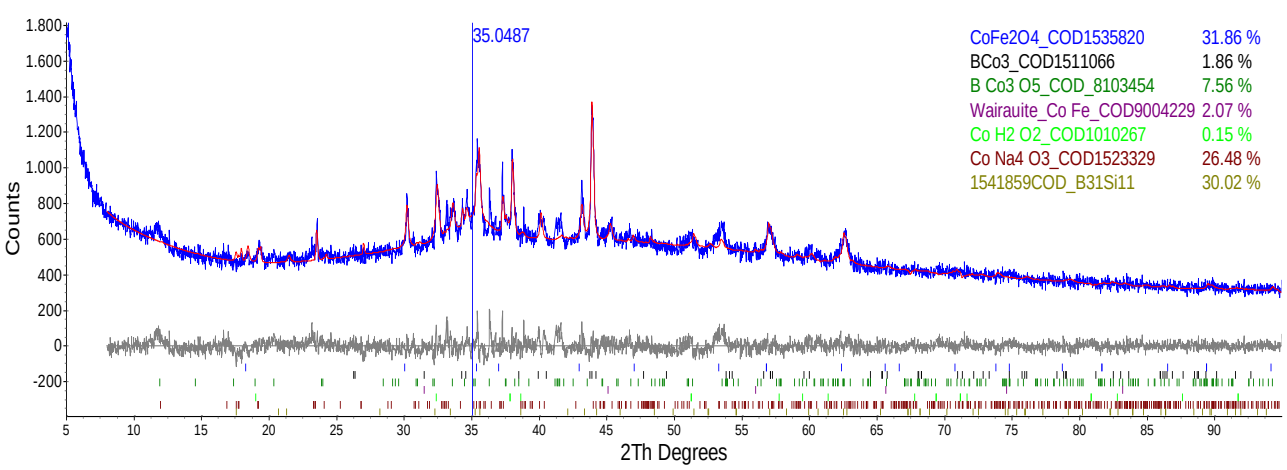

Figure A7. Rietveld preliminary refinement of catalyst after reuse.

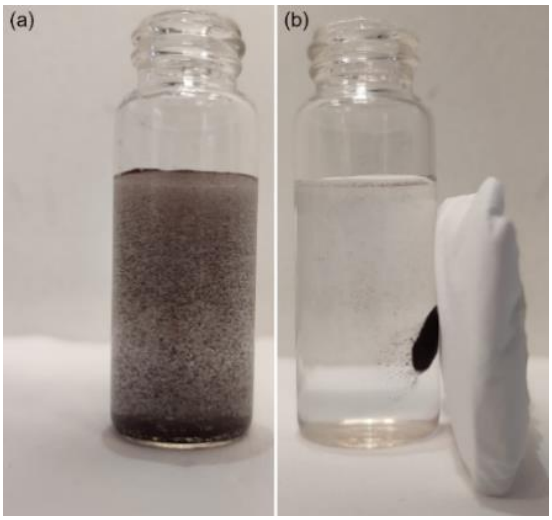

Figure A8. Magnetic response of catalyst sample particles to an external magnetic field: (a) and with exposition to an external magnetic field (b).

NaOH (%w/v)	$NaBH_4$ (%w/v)	Temperature (°C)	H_2 generated in 1 hour (mL)
0	2	25	123.0
1	2	25	2.0
2	2	25	0.0
4	2	25	0.0
2.5	2	55	10.0

Table A1. H_2 generation without catalyst addition under varying NaOH initial concentrations at 25 and 55°C.

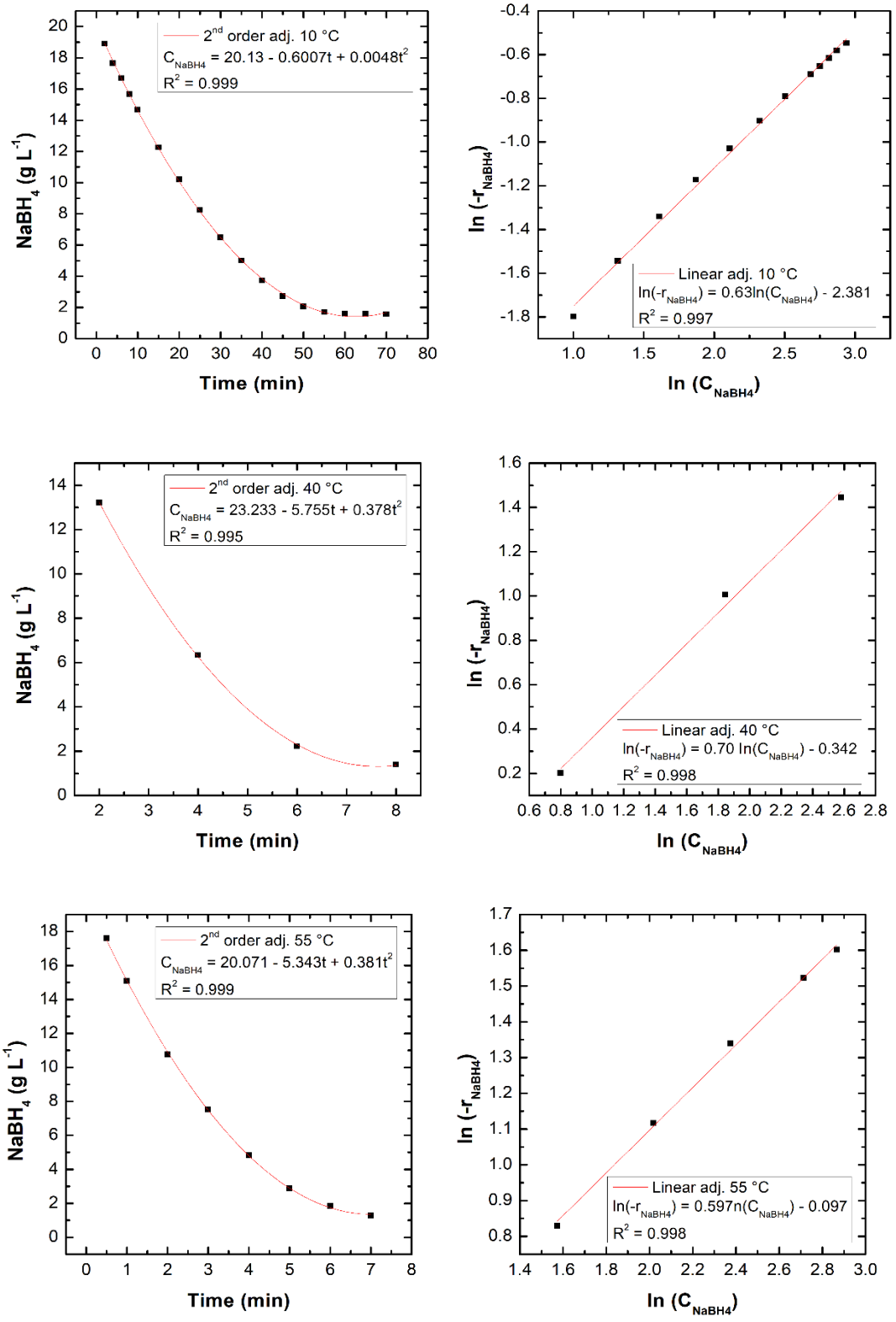

Figure A9. Polynomial fitting and kinetic data linear regression for temperatures 10, 40 and 55°C for for 50 mg catalyst, 2.5% NaOH w/v, 2.0% $NaBH_4$ w/v.

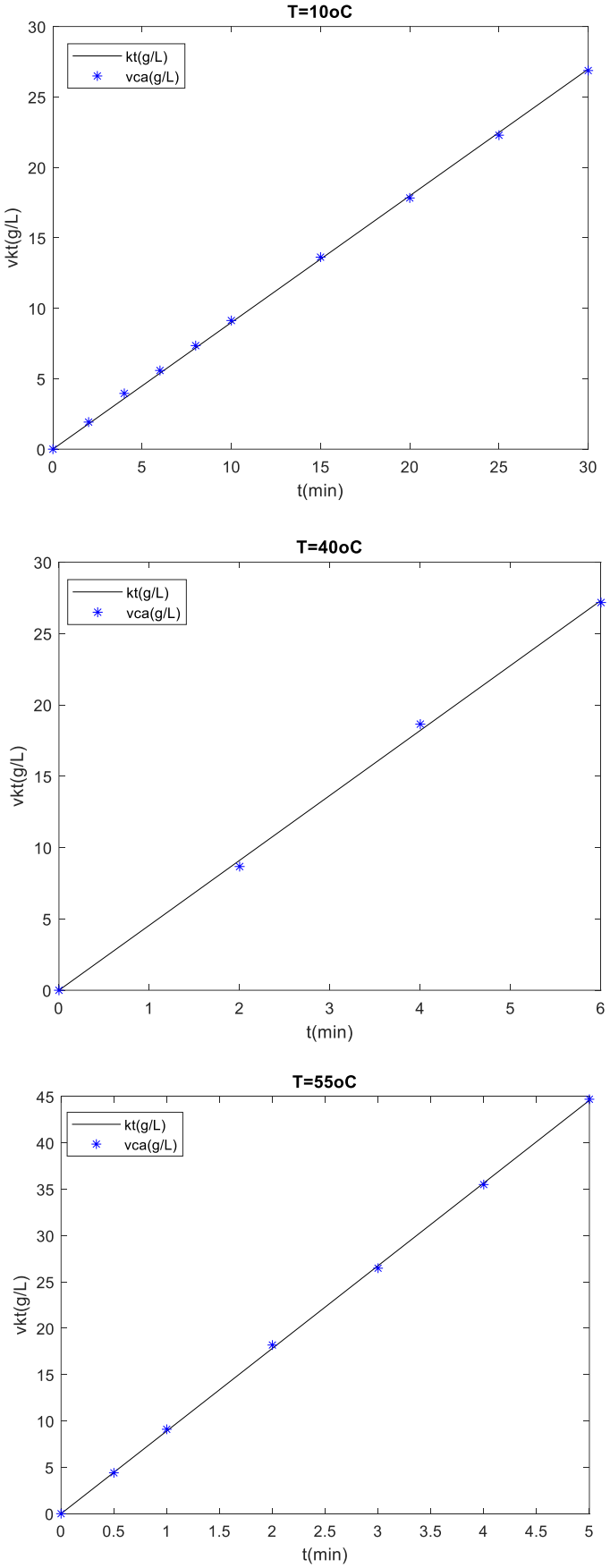

Figure A10. Langmuir – Hischelwood fitting for temperatures at 10°C, 40°C and 55°C for 50 mg catalyst, 2.5% NaOH w/v, 2.0% $NaBH_4$ w/v.

Temperature [°C]	Estimated parameters for empirical model	
10	n	0.63
	k ($g.L^{-1}$ min^{-1})	0.0925
	R^2	0.997
25	n	0.584
	k ($g.L^{-1}$ min^{-1})	0.437
	R^2	0.999
40	n	0.704
	k ($g.L^{-1}$ min^{-1})	0.71
	R^2	0.996
55	n	0.597
	k ($g.L^{-1}$ min^{-1})	0.908
	R^2	0.998

1141 **Table A2.** Estimated parameters for empirical model at 10°C, 25°C, 40°C and 55°C.

Temperature [°C]	Estimated parameters for L-H model	
10	K ($L.g^{-1}$)	0.0852
	k ($g\ L^{-1}$ min^{-1})	0.899
	R^2	0.999
25	K ($L.g^{-1}$)	1.267
	k ($g.L^{-1}$ min^{-1})	1.771
	R^2	
40	K ($L.g^{-1}$)	0.237
	k ($g\ L^{-1}$ min^{-1})	4.553
	R^2	0.999
55	K ($L.g^{-1}$)	0.071
	k ($g\ L^{-1}$ min^{-1})	8.917
	R^2	0.999

1142 **Table A3.** Estimated parameters for L- H model at 10°C, 25°C, 40°C and 55°C.